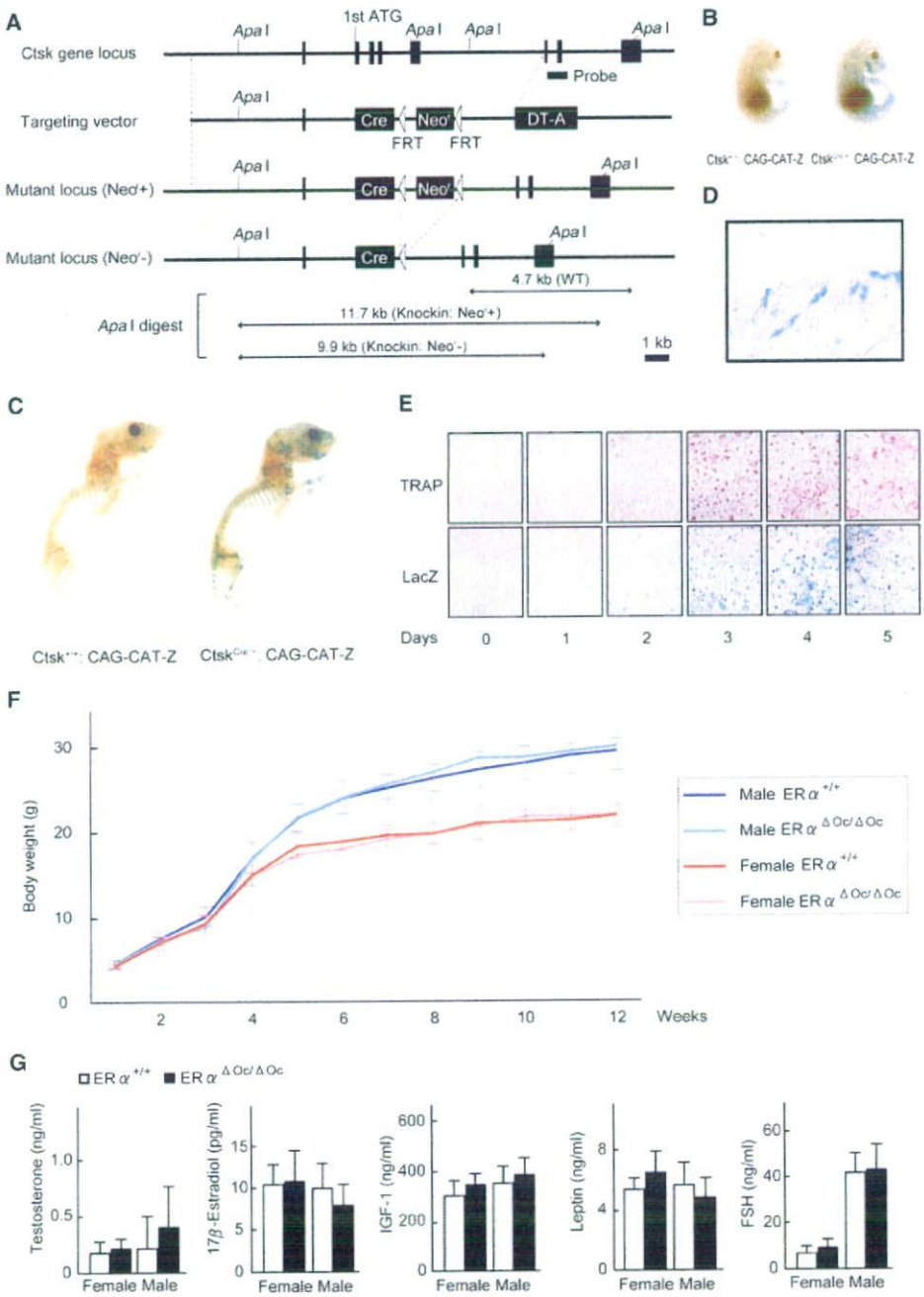

Figure 1. Generation of Knockin Mice Selectively Expressing Cre in Mature Osteoclasts

(A) Illustration of the targeting strategy for insertion of the *Cre* gene into the mouse *Cathepsin K* (*Ctsk*) gene. A targeting vector was generated to contain the *Cre* cDNA at the endogenous ATG start site, followed by a *FRT* (Flp-recombinase target)-flanked *Neo*^{r} cassette. The *DT-A* (diphtheria toxin-A) gene was also inserted to avoid random integrations.

(B and C) *Ctsk-Cre* mice were then crossed with *CAG-CAT-Z* mice. β-galactosidase activity derived from the activated *LacZ* reporter gene was monitored to test if expressed Cre excised the *loxP* sites in mature osteoclasts. LacZ expression patterns reflected the localization patterns of mature osteoclasts in the developing bone at 16.5 days post coitum embryos and in the skeletal tissues of 7-day-old pups.

(D) The LacZ expression induced by Cre-mediated excision was also seen in osteoclasts attached to trabecular bone in the lumber vertebrae of 12-week-old mice.

(E) LacZ expression was induced during osteoclastogenesis. Osteoclast-like cells that differentiated from bone-marrow macrophages following culture in the presence of M-CSF and RANKL were stained with TRAP (tartrate-resistant acid phosphatase), a mature osteoclast marker.

Delmas, 2002; Raisz, 2005; Rodan and Martin, 2000). Estrogen deficiency in postmenopausal women frequently leads to osteoporosis, the most common skeletal disorder. Similarly, ovariectomy clearly produces an osteoporotic bone phenotype in mice. Osteoporotic bone loss is the result of high bone turnover in which bone resorption outpaces bone deposition (Rodan and Martin, 2000; Teitelbaum, 2007). This imbalance in bone turnover that is induced by estrogen deficiency in women and female rodents can be ameliorated with bio-available estrogens including selective estrogen receptor modulators (SERMs) (Riggs and Hartmann, 2003).

Estrogen and SERMs primarily act by regulating gene transcription via estrogen receptors (ERα, ERβ) (Couse and Korach, 1999; Shang and Brown, 2002). ERs belong to the nuclear receptor gene superfamily and act as ligand-inducible transcriptional factors (Mangelsdorf et al., 1995). ER dimers directly or indirectly associate with specific DNA elements in the target gene promoter (Shang and Brown, 2002) and control transcription through reorganizing chromatin structure and histone modifications (Belandia and Parker, 2003). Genetic mouse models (KO mice) lacking ERα ($ER\alpha^{-/-}$) and ERβ ($ER\beta^{-/-}$) provide insights into ER function (Mueller and Korach, 2001; Windahl et al., 2002). In mice, though ERα appears to be the major receptor in most estrogen target tissues including bone (Sims et al., 2003), neither clear bone loss nor high bone turnover is detectable in ERα single or ERα/ERβ double-KO females (Syed and Khosla, 2005; Windahl et al., 2002). This unexpected maintenance of bone mass in female mutants is presumed to be due to unphysiologically elevated levels of other osteoprotective hormones, like androgens. Systemic defects in the hypothalamus caused by ER inactivation appear to impair the negative feedback system of hormone production (Syed and Khosla, 2005). This leads to an excess in estrogen precursors, notably androgens. In fact, the anabolic effects of androgens mediated by the androgen receptor (AR) are evident in female mice (Kawano et al., 2003; Sims et al., 2003). In males, estrogen is also osteoprotective, as is evident by the development of osteopenia in male patients genetically deficient in ERα (Smith et al., 1994) or aromatase activity (Simpson and Davis, 2001). Thus, irrespective of the accumulating clinical and basic research data on the osteoprotective actions of estrogen and SERMs, the molecular basis of this osteoprotection in females remains elusive.

To study the molecular interactions behind the antibone resorptive actions of estrogen in women and female animals, we genetically ablated ERα in mature osteoclasts ($ER\alpha^{\Delta Oc/\Delta Oc}$). Selective ablation of ERα in differentiated osteoclasts ($ER\alpha^{\Delta Oc/\Delta Oc}$) was accomplished by crossing a *Cathepsin K-Cre* knockin mouse with a floxed *ERα* mouse. This resulted in clear trabecular bone loss and high bone turnover associated with increased osteoclast numbers in females but not in males. In the female mutants, further bone loss following ovariectomy was not significant and recovery by estrogen was ineffective in the trabecular areas of long bones and lumbar vertebral bodies. Upregulated expression of *Fas ligand* (*FasL*) gene, and increased apoptosis in differentiated osteoclasts by estrogen was found in the intact bone of wild-type females but undetectable in $ER\alpha^{\Delta Oc/\Delta Oc}$ females. Induction of FasL and apoptosis by estrogen as well as a SERM also required ERα in cultured osteoclasts. Thus, we propose that the osteoprotective actions of estrogen and SERMs are mediated at least in part through osteoclastic ERα in trabecular bone, and the life span of mature osteoclasts is regulated through the activation of the FasL signaling.

RESULTS

Generation of Osteoclast-Specific *ERα* Gene Disruption by Knocked-In *Cre* in the *Cathepsin K* Gene

To specifically disrupt *ERα* gene in mature osteoclasts, we knocked in *Cre* into the gene locus of *Cathepsin K* ($Ctsk^{Cre/+}$) (Figures 1A, S1A, and S1B), a gene known to be expressed in differentiated osteoclastic cells arising from hematopoietic stem cells. This gene is functionally indispensable for mature osteoclasts (Saftig et al., 1998). Only one copy appears enough to support normal bone formation and bone turnover, since heterozygous mutant mice of *Cathepsin K* ($Ctsk^{+/-}$) have no obvious bone phenotype (Gowen et al., 1999; Li et al., 2006; Saftig et al., 1998) . Clear, bone-specific expression of the *Cre* transcript in the adult $Ctsk^{Cre/+}$ mice was observed in the tested tissues (Figure S1C). To confirm Cre protein expression, the $Ctsk^{Cre/+}$ mice were crossed with tester mice (*CAG-CAT-Z*). These mice were genetically engineered to express β-galactosidase by excision of the transcribed stop sequence in front of the *β-galactosidase* gene (*LacZ*) in cells expressing Cre (Sakai and Miyazaki, 1997). β-galactosidase expression visualized by LacZ staining was observed in the bones of 16.5 dpc embryos and 7-day-old pups of $Ctsk^{Cre/+}$; *CAG-CAT-Z* mice. Expression patterns were consistent with the appearance and skeletal localization of functionally mature osteoclasts (Figures 1B and 1C). Histochemical staining of LacZ in the lumbar vertebrae of 12-week-old mice was localized in multinuclear osteoclasts (Figure 1D) but not seen in osteoblasts and osteocytes (Figure S1D) and the hypothalamus (Figure S1E). Since *Cathepsin K* gene expression is evident in differentiated osteoclasts (Saftig et al., 1998), we used an in vitro culture cell system to test whether Cre expression was driven by the endogenous promoter that is induced at the time of osteoclast differentiation. Osteoclast-precursor cells derived from bone marrow

(F) The growth curve of $ER\alpha^{\Delta Oc/\Delta Oc}$ mice was indistinguishable from that of the control mice. Data are represented as mean ± SEM.
(G) Serum hormone levels were normal in 12-week-old $ER\alpha^{\Delta Oc/\Delta Oc}$ (filled column) versus $ER\alpha^{+/+}$ (open column) mice (n = 10–11 animals per genotype). Data are represented as mean ± SEM.

were cytodifferentiated for 1 week in the presence of M-CSF (macrophage colony stimulating factor) and RANKL (receptor activator of NFκB ligand) (Koga et al., 2004). TRAP-positive osteoclasts emerged after 3 days of culture (Figure 1E). The number of TRAP-positive osteoclasts and the number of LacZ-expressing cells simultaneously increased. In the contrast, the LacZ expression was not detected in primary cultured osteoblasts derived from the calvaria (Figure S1F). In view of both our in vivo and in vitro observations, we conclude that the $Ctsk^{Cre/+}$ mouse line expresses Cre in differentiated osteoclasts. Moreover, estrogen response in bone mass control was not distinguishable in between $Ctsk^{Cre/+}$ and $Ctsk^{+/+}$ mice (Figure S2A).

We then crossed floxed $ER\alpha$ mice (Dupont et al., 2000) with $Ctsk^{Cre/+}$ mice to disrupt ERα in differentiated osteoclasts ($ER\alpha^{\Delta Oc/\Delta Oc}$). Excision of the $ER\alpha$ gene (Figure S1G) was confirmed by Southern blotting of DNA from adult female and male (data not shown) bone as well as in cultured mature osteoclasts (Figure S1H). No overt differences were observed in the growth curve, reproduction, or tissues for up to 12 weeks of age (Figure 1F) between the $Ctsk^{Cre/+}$; $ER\alpha^{+/+}$ ($ER\alpha^{+/+}$) and the $Ctsk^{Cre/+}$; $ER\alpha^{flox/flox}$ ($ER\alpha^{\Delta Oc/\Delta Oc}$) mice, with the exception of the female bones. Serum levels of sex hormones and bone remodeling regulators such as IGF-I, leptin, and follicle-stimulating hormone (Sun et al., 2006; Takeda et al., 2002) appeared unchanged in both male and female $ER\alpha^{\Delta Oc/\Delta Oc}$ mice at 12 weeks (Figure 1G).

Osteopenia Occurred in Osteoclast-Specific ERα KO Females But Not Males

The 12-week-old $ER\alpha^{\Delta Oc/\Delta Oc}$ females exhibited a clear reduction in bone mineral density (BMD) in the femurs (Figures 2A–2C) and tibiae (data not shown) when compared with $ER\alpha^{+/+}$ mice. Though cortical bone appeared unaffected, trabecular bone loss (Figure 2A) with significant reduction of trabecular bone volume (BV/TV) (Figure 2F) was clearly seen. This is similar to the osteoporotic abnormalities observed in women during natural menopause or following ovariectomy (Delmas, 2002; Tolar et al., 2004). However, unlike men deficient in aromatase or ERα activity (Simpson and Davis, 2001; Smith et al., 1994), $ER\alpha^{\Delta Oc/\Delta Oc}$ males unexpectedly exhibited no clear bone loss even in the trabecular areas (Figures 2A–2C). In $ER\alpha^{\Delta Oc/\Delta Oc}$ females, both the bone-formation rate, estimated by double-calcein labeling (Figure 2D), as well as the bone-resorption rate, estimated from TRAP-positive differentiated osteoclast numbers (Figure 2E), were increased, indicating high bone turnover. Histomorphometric analyses of $ER\alpha^{\Delta Oc/\Delta Oc}$ females supported the observation of accelerated bone resorption, as increased numbers of osteoclasts (Oc. S/BS and N. Oc/BS) were observed together with more eroded bone surface (ES/BS in Figure 2F). Bone formation was also enhanced as the rates of mineral apposition (MAR) and bone formation (BFR/BS) were both upregulated without an increase in osteoblast numbers (Ob.S/BS) (Figure 2F). Thus, considering all of these findings, it is conceivable that the increased number of differentiated osteoclasts following ERα ablation accelerates bone resorption over formation, leading to bone loss in the trabecular areas.

No Further Bone Loss Results from Estrogen Deficiency in $ER\alpha^{\Delta Oc/\Delta Oc}$ Females

To verify whether osteoclastic ERα indeed mediates osteoprotective estrogen actions, estrogen action was investigated by ovariectomy (OVX) of 12-week-old female mice. As expected, OVX in $ER\alpha^{+/+}$ females resulted in significantly reduced BMD particularly in the trabecular bone (Figures 3A and 3B) but not in the cortical bone (Figure 3C). Consistent with previous reports, (Kimble et al., 1995; Teitelbaum and Ross, 2003), estrogen deficiency following OVX upregulated the serum levels of cytokines like TNFα and IL-1α (Figure 3D). These cytokines enhance bone resorption through stimulation of osteoclastogenesis, leading to the loss of bone mass (Teitelbaum and Ross, 2003). OVX did not further reduce BMD or trabecular bone volume of the femurs of $ER\alpha^{\Delta Oc/\Delta Oc}$ females (Figure 3B) nor affect increased number of TRAP-positive osteoclasts (see lower panel in Figure 3A) despite upregulation of serum cytokines. This suggests that the expression of cytokines known to regulate bone resorption is not under the control of osteoclastic ERα.

Estrogen Treatment Failed to Rescue the Osteoporotic Bone Phenotype of $ER\alpha^{\Delta Oc/\Delta Oc}$ Mice

Estrogen treatment by estrogen pellet implantation (OVX + E2) for 2 weeks after OVX in $ER\alpha^{+/+}$ mice elicited a dramatic increase in bone mass in both the trabecular and cortical areas of the femurs (data not shown) and lumbar vertebral bodies (Figure 4A). Estrogen action during E2 treatment in female mutants ($ER\alpha^{\Delta Oc/\Delta Oc}$) was not as pronounced as in the $ER\alpha^{+/+}$ females (Figures 4A and 4B), and the increase in the trabecular portions of the distal femurs was slight (data not shown). Histomorphometric analysis of the lumbar vertebral bodies (Figure 4B) supported the idea that E2 treatment in the female mutants was not sufficient to suppress accelerated bone resorption. These in vivo findings in the $ER\alpha^{\Delta Oc/\Delta Oc}$ females suggest that in at least the trabecular areas of the long bones and lumbar vertebral bodies, the osteoprotective estrogen action is primarily mediated via osteoclastic ERα inhibiting bone resorption.

To further test this hypothesis, we investigated ERα protein expression in mature osteoclasts from trabecular bone. Few reports document osteoclastic expression of ERα protein and an estrogen response in both intact animals and in in vitro cultured osteoclasts (Bland, 2000). We therefore reasoned that ER expression ceases during differentiation into mature cells from primary cultures of osteoclast precursors, similar to that observed in other primary culture cell systems such as avian oviduct cells, in which ERα protein expression is drastically decreased during culture (Kato et al., 1989). Using highly sensitive immunohistochemistry, we investigated whether

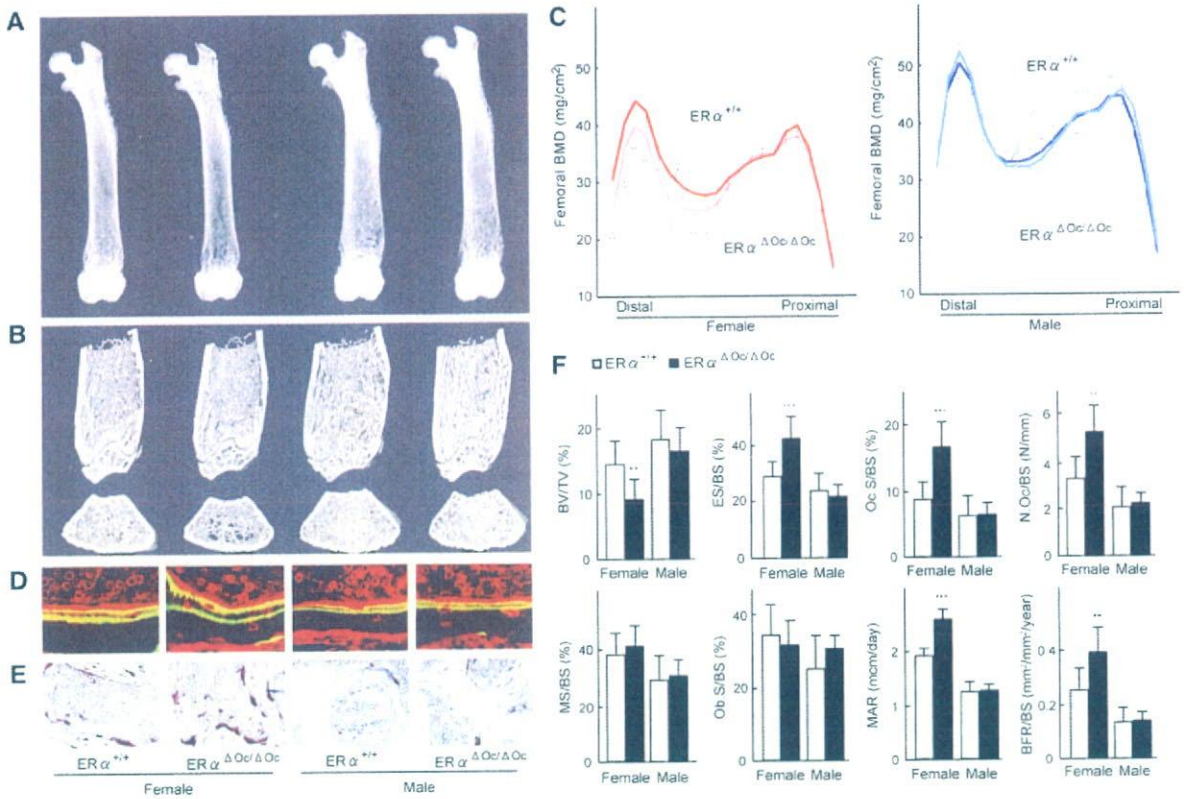

Figure 2. High Bone Turnover Osteopenia Was Observed in $ER\alpha^{\Delta Oc/\Delta Oc}$ Females But Not Males

(A) Soft X-ray images of femurs from 12-week-old $Ctsk^{Cre/+}$; $ER\alpha^{flox/flox}$ ($ER\alpha^{\Delta Oc/\Delta Oc}$) mice.

(B) Three-dimensional computed tomography images of the distal femurs and axial sections of distal metaphysis from representative 12-week-old $Ctsk^{Cre/+}$; $ER\alpha^{+/+}$ ($ER\alpha^{+/+}$) and $ER\alpha^{\Delta Oc/\Delta Oc}$ mice.

(C) BMD of each of 20 equal longitudinal divisions of femurs from 12-week-old $ER\alpha^{+/+}$ and $ER\alpha^{\Delta Oc/\Delta Oc}$ mice. (n = 10–11 animals per genotype; Student's t test, $^*p < 0.05$; $^{**}p < 0.01$; $^{***}p < 0.001$). Data are represented as mean ± SEM.

(D) Bone formation was also accelerated in $ER\alpha^{\Delta Oc/\Delta Oc}$ females when two calcein-labeled mineralized fronts visualized by fluorescent micrography were measured in the proximal tibia of 12-week-old mice.

(E) The number of TRAP-positive osteoclasts in the lumbar spine of female mice was increased by selective disruption of ERα in osteoclasts, indicating enhanced bone resorption.

(F) Bone turnover parameters as measured by dynamic bone histomorphometry after calcein labeling indicated high bone turnover in $ER\alpha^{\Delta Oc/\Delta Oc}$ females. Parameters are measured in the proximal tibia of 12-week-old $ER\alpha^{+/+}$ (open column) and $ER\alpha^{\Delta Oc/\Delta Oc}$ (filled column) mice. BV/TV: bone volume per tissue volume. ES/BS: eroded surface per bone surface. Oc.S/BS: osteoclast surface per bone surface. N.Oc/BS: osteoclast number per bone surface. MS/BS: mineralizing surface per bone surface. Ob.S/BS: osteoblast surface per bone surface. MAR: mineral apposition rate. BFR/BS: bone formation rate per bone surface (n = 10–11 animals per genotype; Student's t test, $^*p < 0.05$; $^{**}p < 0.01$; $^{***}p < 0.001$). Data are represented as mean ± SEM.

ERα protein expresses in differentiated osteoclasts in the bone tissues of femur sections from 12-week-old mice. ERα protein expression appeared abundant in osteoblasts and osteocytes of femur sections (Figure 4C) as well as hypothalamus (Figure S2B) from 12-week-old mice, in agreement with a previous report (Zaman et al., 2006). Likewise, expression levels of ERα in primary cultured osteoblasts derived from calvaria of $ER\alpha^{\Delta Oc/\Delta Oc}$ females appeared unaffected (Figure S2C). In contrast, in differentiated osteoclasts of the same femur sections, ERα expression was definitely detectable but very low in the $ER\alpha^{+/+}$ but undetectable in $ER\alpha^{\Delta Oc/\Delta Oc}$ females (Figure 4C).

Signaling by Osteoclastogenic Factors and Osteoclastogenesis Is Intact in Osteoclasts Deficient in ERα

It is possible that the osteoprotective function of osteoclastic ERα inhibits osteoclastogenesis. To address this issue, osteoclastogenesis was tested in cultured osteoclasts derived from bone-marrow cells of $ER\alpha^{\Delta Oc/\Delta Oc}$ mutants. In this cell culture system, a possible contribution of contaminated immune cells and stromal cells could be excluded, since osteoclastogenesis is only inducible by M-CSF treatment followed by M-CSF + RANKL (Koga et al., 2004).

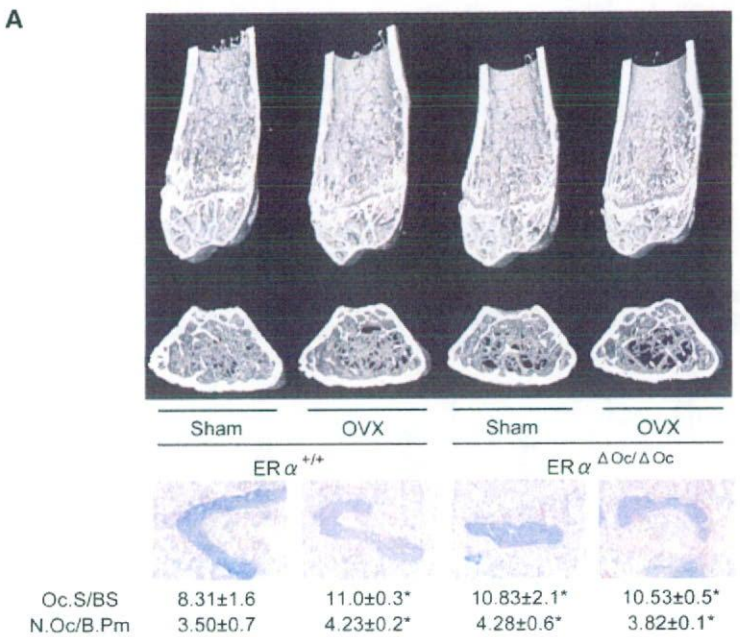

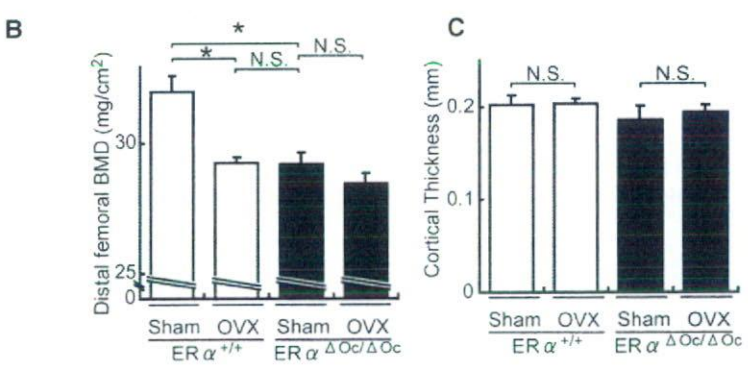

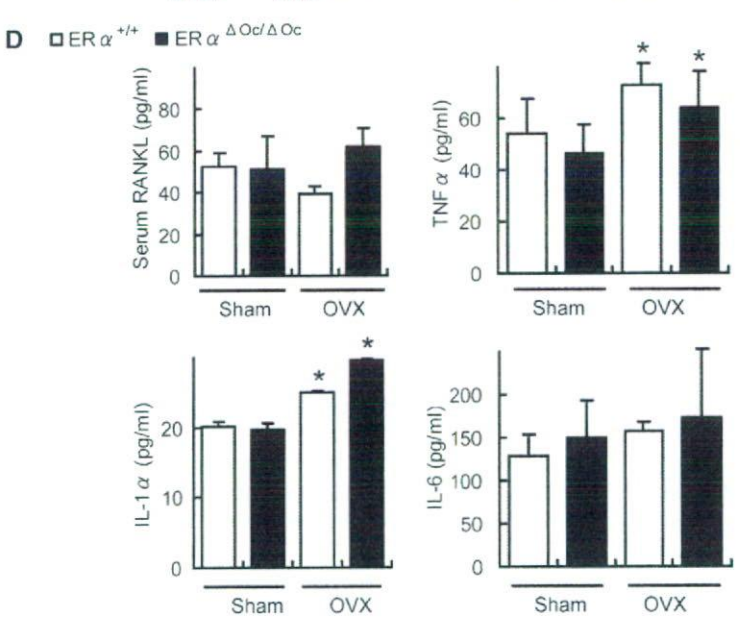

Figure 3. No Further Bone Loss of $ER\alpha^{\Delta Oc/\Delta Oc}$ Females by Ovariectomy

(A) Distal femoral micro CT analysis and lumbar vertebral bone histomorphometrical analysis of sham-operated or ovariectomized (OVX) 12-week-old $ER\alpha^{+/+}$ and $ER\alpha^{\Delta Oc/\Delta Oc}$ mice (*$p < 0.05$ compared to $ER\alpha^{+/+}$ sham group). Two weeks after OVX, the bone phenotype was analyzed.

(B) BMD of the distal femurs within each group are described in Figure 3A (*$p < 0.05$; N.S., not significant). Data are represented as mean ± SEM.

(C) Cortical thickness evaluation from micro CT analysis of femurs within each group described in Figure 3A. Data are represented as mean ± SEM.

(D) The levels of TNFα, IL-1α, and IL-6 in the bone-marrow cells culture media and serum RANKL (*$p < 0.05$ compared to each sham group). Data are represented as mean ± SEM.

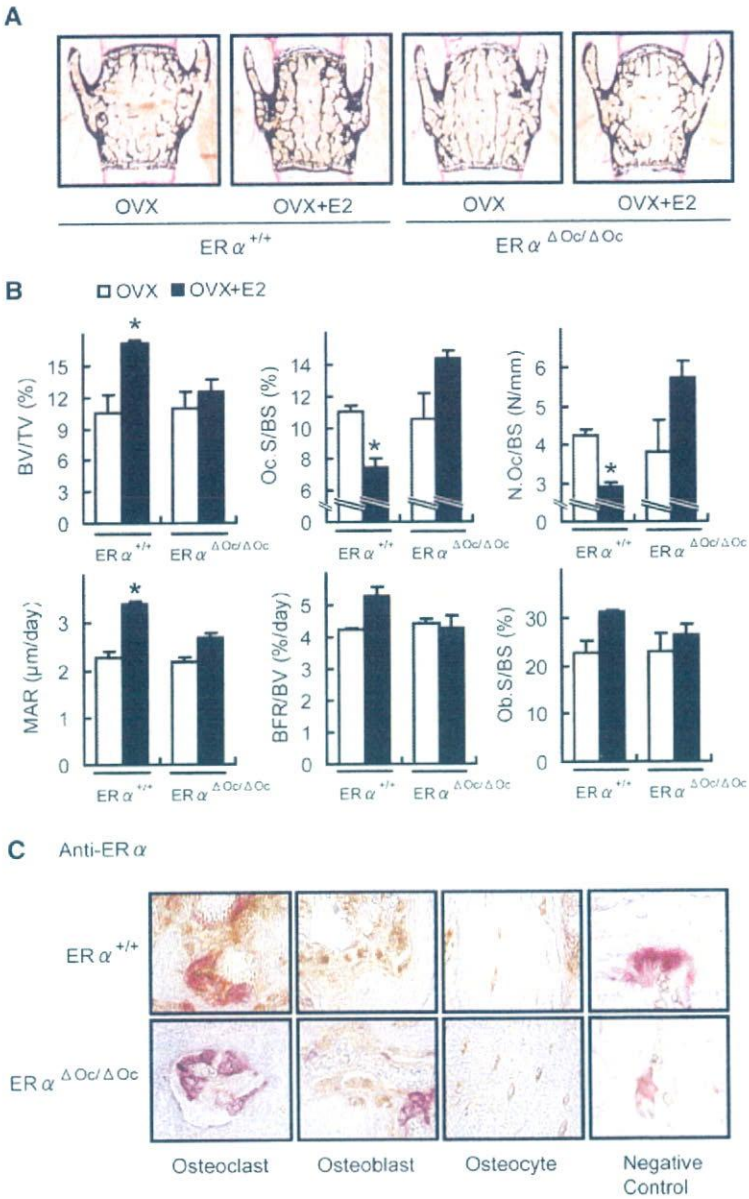

Figure 4. Estrogen treatment failed to reverse trabecular bone loss of ovariectomized $ER\alpha^{\Delta Oc/\Delta Oc}$ females

(A) von kossa staining of lumbar vertebral bodies of ovariectomized $ER\alpha^{+/+}$ and $ER\alpha^{\Delta Oc/\Delta Oc}$ mice treated with or without 17β-estradiol (0.83 μg/day) for 2 weeks (+E2) groups.

(B) Bone histomorphometrical analyses of the lumber vertebral bodies of 12-week-old ovariectomized $ER\alpha^{+/+}$ (left columns) and $ER\alpha^{\Delta Oc/\Delta Oc}$ (right columns) mice with (filled columns) or without (open columns) E2 treatment for 2 weeks (*$p < 0.05$ compared with E2-treated ovariectomized $ER\alpha^{\Delta Oc/\Delta Oc}$ mice). BV/TV: bone volume per tissue volume. ES/BS: eroded surface per bone surface. Oc.S/BS: osteoclast surface per bone surface. N.Oc/BS: osteoclast number per bone surface. MS/BS: mineralizing surface per bone surface. Ob.S/BS: osteoblast surface per bone surface. MAR: mineral apposition rate. BFR/BS: bone formation rate per bone surface. Data are represented as mean ± SEM.

(C) Immunochemical identification of ERα (brown) in TRAP-positive (red) differentiated osteoclasts. The femurs of 12 week-old mice were used for the immunodetection of ERα in bone cells. All labels were abolished when the primary antibody was preadsorbed with the immunizing peptide (negative control).

The number of TRAP-positive osteoclasts differentiated from the bone-marrow cells of $ER\alpha^{\Delta Oc/\Delta Oc}$ females was almost the same as that from $ER\alpha^{+/+}$ females (Figure 5A) and males (data not shown). The differentiated $ER\alpha^{\Delta Oc/\Delta Oc}$ osteoclasts had typical osteoclastic features, including the characteristic cell shape, TRAP-positive, multiple nuclei, and actin-ring formation, and were indistinguishable from the $ER\alpha^{+/+}$ osteoclasts (Figure 5B).

The expression levels of the prime osteoclastogenic transcription factors, c-*fos* and *NFATc1*, were unaltered by ERα deficiency in differentiated osteoclasts (Figure 5C). Furthermore, responses to RANKL in intracellular signaling, as represented by phosphorylation of p38 and IκB, were unaffected in $ER\alpha^{\Delta Oc/\Delta Oc}$ osteoclasts from females (Figure 5D) as well as males (data not shown). In light of these findings, it is unlikely that activated ERα in osteoclastic cells attenuates osteoclastogenesis.

Activation of the Fas/FasL System by Estrogen in Intact Bone Is Impaired by Osteoclastic ERα Deficiency

To examine osteoclastic ERα function in intact bone, DNA microarray analysis following real-time RT-PCR of RNA from the femurs of ovariectomized $ER\alpha^{\Delta Oc/\Delta Oc}$ females treated with or without estrogen, was performed. During

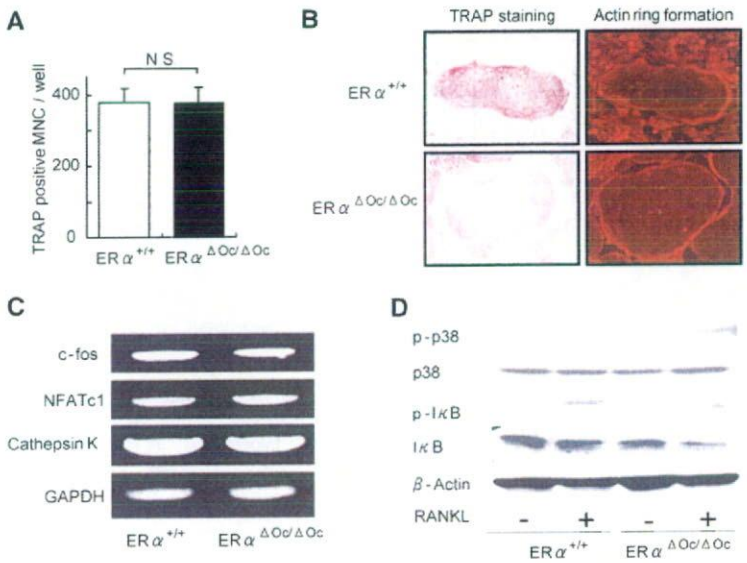

Figure 5. ERα Deficiency Did Not Affect Osteoclastogenesis

(A) TRAP-positive multinucleated cell count at 3 days after RANKL stimulation, cultured in 24-well plates (n = 6, N.S., not significant). Data are represented as mean ± SEM.

(B) TRAP staining and actin ring formation of RANKL induced primary cultured osteoclasts from bone-marrow cells of $ER\alpha^{+/+}$ and $ER\alpha^{\Delta Oc/\Delta Oc}$ mice.

(C) RT-PCR analysis of genes related to osteoclastogenesis.

(D) Western blot analysis of phosphorylated p38, JNK, and IκB of primary cultured bone-marrow cells stimulated with or without 100 ng/ml of RANKL for 15 min.

the search for candidate ERα target genes in bone by DNA microarray analysis (Figure S3), we found that a number of apoptosis-related factors were regulated by estrogen in the intact bone of $ER\alpha^{+/+}$ females but dysregulated in $ER\alpha^{\Delta Oc/\Delta Oc}$ females. This observation is consistent with a previous report of estrogen-induced apoptosis of mature osteoclasts (Kameda et al., 1997). Real-time RT-PCR to validate the estrogen regulations of the candidate genes revealed that gene expression of *FasL*, an apoptotic factor, was responsive to E2 (Figure 6A). Estrogen treatment (+E2) indeed induced expression of FasL protein in bone of ovariectomized $ER\alpha^{+/+}$, but this induction was not obvious in ovariectomized $ER\alpha^{\Delta Oc/\Delta Oc}$ mice (Figures 6B and 6C). Reflecting FasL induction by estrogen, estrogen-induced apoptosis (as observed by the TUNEL assay) in TRAP-positive mature trabecular osteoclasts in the distal femurs of the $ER\alpha^{+/+}$ mice was detected, but this E2 response was abolished in the $ER\alpha^{\Delta Oc/\Delta Oc}$ mice (Figure 6D). Furthermore, in mice lacking functional FasL ($FasL^{gld/gld}$), neither enhanced bone resorption nor bone mass loss was induced by ovariectomy (Figures 6E and 6F).

Osteoclastic ERα Mediates Estrogen-Induced apoptosis by FasL

The expression level of ERα protein in differentiated osteoclasts derived from bone marrow cells was very low, but induction of *FasL* gene expression was also detectable in the cultured osteoclasts of $ER\alpha^{+/+}$ females as well as males (Figure 7A). However, this E2 response was impaired in cultured osteoclasts from $ER\alpha^{\Delta Oc/\Delta Oc}$ females (Figure 7A). It is notable that such responses are also induced by tamoxifen (Figure 7C), which is an osteoprotective SERM (Harada and Rodan, 2003). ERα overexpression augmented *FasL* gene expression in response to estrogen in cultured osteoclasts from $ER\alpha^{\Delta Oc/\Delta Oc}$ females (Figure S4A). In primary cultured calvarial osteoblasts from females as well as males (Suzawa et al., 2003), *FasL* gene induction by E2 and tamoxifen was also seen; however, it was not accompanied by increased apoptosis (data not shown). Thus, it appears that estrogen-induced apoptosis in osteoclasts is mediated by FasL expression in osteoclasts in the trabecular bone areas, presumably as well as in osteoblasts in cortical bone areas. As expected, the cell number of TUNEL-positive osteoclasts was increased by E2 in the cultured osteoclasts from $ER\alpha^{+/+}$ females, but E2-induced apoptosis was undetectable in $ER\alpha^{\Delta Oc/\Delta Oc}$ osteoclasts (Figure 7B). Consistent with FasL-induced apoptosis, *Fas* gene expression was observed (Figure 7D), but it was likely that Fas expression did not require ERα function (Figures S4B and S4C). Expression levels of *Fas* and *ERα* as well as E2 response in apoptosis appeared to fluctuate during osteoclast differentiation (Figures S4B–S4D); however, in FasL mutant ($FasL^{gld/gld}$) females, the E2-induced apoptosis was abolished (Figure S4E). These findings suggest that activated ERα in differentiated osteoclasts induces apoptosis through activating FasL/Fas signaling. This leads to suppression of bone resorption through truncating the already short life span of differentiated osteoclasts (Teitelbaum, 2006).

DISCUSSION

Selective ablation of ERα in mature osteoclasts in female mice shows that the osteoprotective effect of estrogen is mediated by osteoclastic ERα, at least in the trabecular regions of the tibiae, femur, and lumbar vertebrae of female mice. Activated ERα by estrogen as well as SERMs appears to truncate the already short life span (estimated at 2 weeks) of differentiated osteoclasts by inducing apoptosis through activation of the Fas/FasL system.

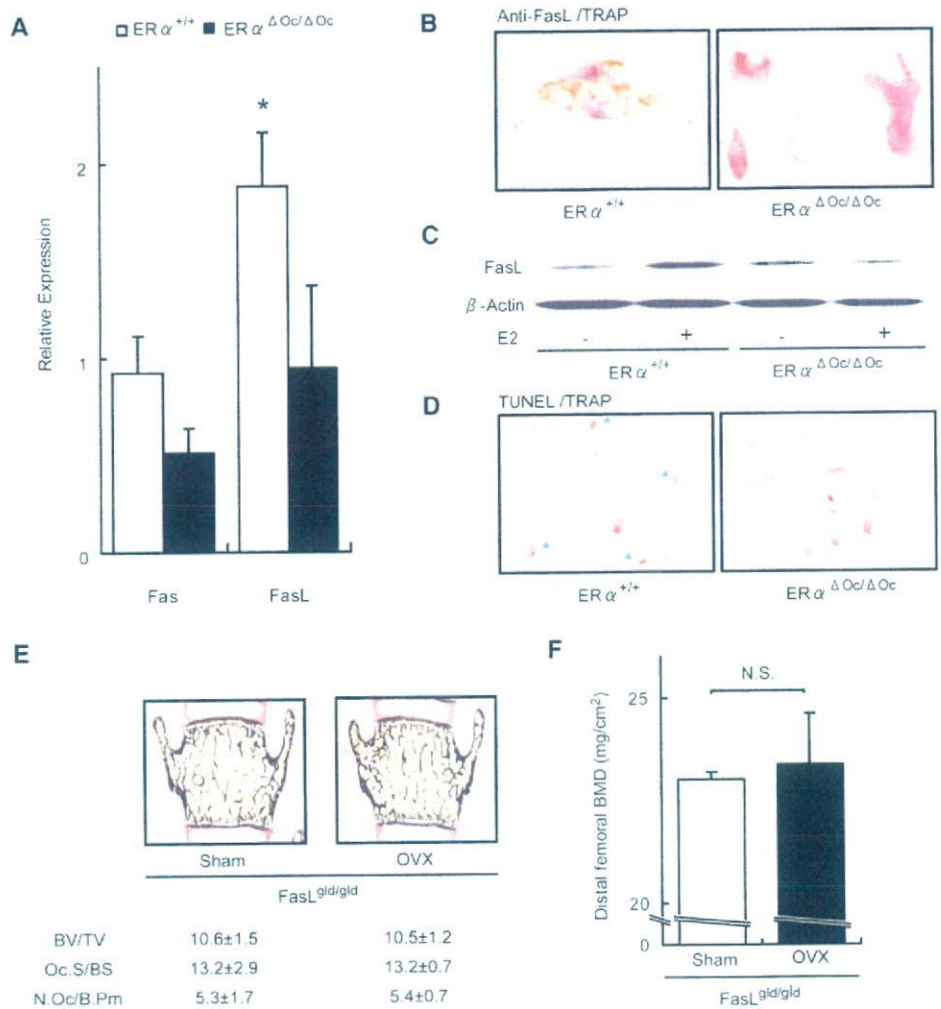

Figure 6. Activated ERα Induced Fas Ligand Expression and Apoptosis in Differentiated Osteoclasts of Intact Bone

(A) Real-time RT-PCR analysis of *Fas* and *FasL*. Expression levels in bones from E2-treated ovariectomized $ER\alpha^{+/+}$ (open column) and $ER\alpha^{\Delta Oc/\Delta Oc}$ (filled column) were compared with the ovariectomized groups of each genotype without E2 administration (*$p < 0.05$ compared to $ER\alpha^{+/+}$). Data are represented as mean ± SEM.

(B) Immunohistochemical analysis of anti-FasL with TRAP staining of the sections from the distal femurs of E2-treated ovariectomized $ER\alpha^{+/+}$ and $ER\alpha^{\Delta Oc/\Delta Oc}$ mice. Brawny stained cells are anti-FasL positive.

(C) Anti-FasL western blot analysis of proteins obtained from femurs of ovariectomized $ER\alpha^{+/+}$ and $ER\alpha^{\Delta Oc/\Delta Oc}$ mice treated with or without E2, using anti-β-actin as internal control.

(D) TUNEL staining with TRAP staining of the sections from the distal femurs of E2-treated ovariectomized $ER\alpha^{+/+}$ and $ER\alpha^{\Delta Oc/\Delta Oc}$ mice. Arrowheads indicate both TUNEL (brown)- and TRAP-positive staining cells.

(E) Bone histomorphometrical analysis of sham-operated or ovariectomized $FasL^{gld/gld}$ mice.

(F) BMD of the distal femurs of sham operated or ovariectomized $FasL^{gld/gld}$ mice. Data are represented as mean ± SEM.

This attenuates bone resorption. This idea is supported by previous observations that estrogen deficiency following menopause or ovariectomy leads to high bone turnover, particularly in the trabecular areas, as bone is rapidly lost through enhanced resorption (Delmas, 2002; Tolar et al., 2004). Thus, estrogen treatment leads to recovery from osteopenia by reducing resorption (Delmas, 2002; Rodan and Martin, 2000), partly by the induction of osteoclast cell death.

In contrast to the osteopenia seen in the $ER\alpha^{\Delta Oc/\Delta Oc}$ females, the $ER\alpha^{\Delta Oc/\Delta Oc}$ male mice unexpectedly had no bone loss. The male mice still demonstrated an ERα-mediated induction of FasL in response to estrogen with subsequent apoptosis of osteoclasts (Figure 7). Both male mice with a deficiency of aromatase that are unable to locally produce estrogen from testosterone and men with a genetic mutation in the *ERα* gene suffer from osteoporosis (Smith et al., 1994). Considering that the

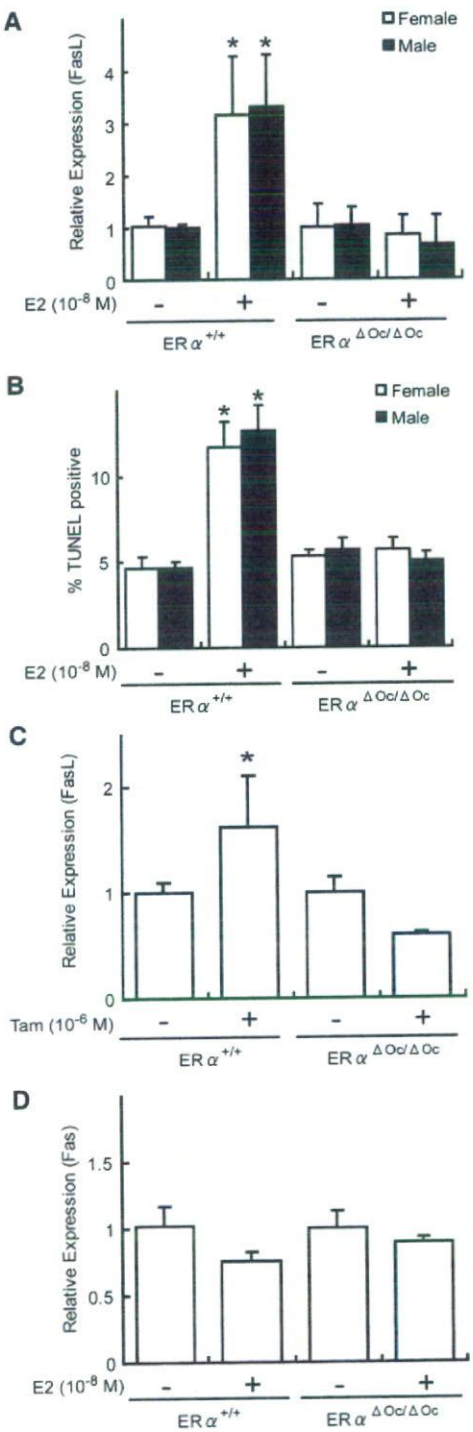

Figure 7. Estrogen-Induced *FasL* Expression and Apoptosis Required ERα in Cultured Osteoclasts

(A) Real-time RT-PCR analysis of *FasL* expression using total RNA obtained from in vitro primary cultured osteoclasts of each genotype at 3 days after RANKL stimulation, treated with or without E2 (10^{-8} M) for 4 hr (*$p < 0.05$ compared to the group treated without E2). Data are represented as mean ± SEM.

(B) Apoptotic cells were defined as those with TUNEL-positive nuclei among TRAP-positive multinucleated primary cultured osteoclasts treated with or without E2 (10^{-8} M) for 12 hr in 96-well plates (*$p < 0.05$ compared to the group treated without E2). Data are represented as mean ± SEM.

(C) *FasL* expression in each genotypic female osteoclastic cells treated with or without Tam (10^{-6} M) (*$p < 0.05$ compared to the group treated without Tam). Data are represented as mean ± SEM.

(D) Expression of *Fas* was measured as described in the legend of Figure 7A. Data are represented as mean ± SEM.

markedly elevated levels of testosterone in ERα KO females may be potent enough to maintain normal bone turnover (Syed and Khosla, 2005), it is likely that the activated AR might be functionally sufficient in male mice to compensate for the ERα deficiency in bone (Kawano et al., 2003). However, species differences in the osteoprotective action of sex steroid hormones still need to be carefully addressed.

Fas/FasL system-mediated apoptotic induction of osteoclasts by estrogen may well be a part of the mechanism for the antiresorptive action of estrogen and SERMs in trabecular bone areas (Delmas, 2002; Rodan and Martin, 2000; Simpson and Davis, 2001; Syed and Khosla, 2005; Tolar et al., 2004). Regulation of osteoclast differentiation is tightly coupled to osteoblastic function in terms of cytokine production and cell-cell contact (Karsenty and Wagner, 2002; Martin and Sims, 2005; Mundy and Elefteriou, 2006; Teitelbaum and Ross, 2003). Indeed, upregulation of osteoclastogenic cytokines by ovariectomy was unaffected in $ER\alpha^{\Delta Oc/\Delta Oc}$ females. Considering the observation that cortical bone mass is increased in ovariectomized $ER\alpha^{\Delta Oc/\Delta Oc}$ females during estrogen treatment, it is conceivable that the antiresorptive estrogen action in cortical bone is also mediated by osteoblastic ERα. In this regard, FasL induction by estrogen in osteoblasts may contribute to the osteoprotective estrogen action, and *FasL* gene induction by estrogen was in fact detected in primary cultured osteoblasts from female calvaria by us as well as another group (S. Krum and M. Brown, personal communication). Thus, similar experiments in which ERα is selectively ablated in osteoblasts are needed to define the role of ERα in these cells.

In osteoclastic cells, expression of the *FasL* gene, which leads to apoptosis, appears to be positive controlled by activated ERα. Not surprisingly, a direct binding site for ERα has been mapped in the *FasL* gene locus (S. Krum and M. Brown, personal communication). An osteoclast- and cell-differentiation stage-specific mechanism may underlie this gene induction in the *FasL* gene promoter. A recent study demonstrated that ERα recruitment to specific promoter sites of given ERα target genes was cell-type specific (Carroll et al., 2005). Thus, there is significant impetus to identify the osteoclastic factor that associates with ERα in the *FasL* gene promoter. Such identification will lead to a better understanding of the molecular basis of the osteoprotective estrogen action and provide a target against which to develop SERMs of greater effectiveness.

EXPERIMENTAL PROCEDURES

Ctsk-Cre Construction and Generation of the Knockin Mouse Lines

An RP23-422n18 BAC clone containing the mouse *Ctsk* gene was purchased from Invitrogen (Carlsbad, CA). The *FRT-Kan^r/Neo^r-FRT* and *nlsCre* fragments were obtained from plasmids pSK2/3-*FRT-Neo* and pIC-*Cre*. Two homologous arms of 500 bp from the *Ctsk* gene were inserted into both sides of the *nlsCre-FRT-Kan^r/Neo^r-FRT* cassette in the pSK2/3-*FRT-Neo* plasmid. The *nlsCre-FRT-Kan^r/Neo^r-FRT* cassette was introduced into the endogenous ATG start site of the *Ctsk* gene by recombineering approaches (Copeland et al., 2001). Targeted BAC was reduced in size from 189 kb to 26 kb and subcloned into the pMC1-DTpA vector by the gap-repair method. The targeted TT2 ES clones were selected after positive-negative selection with G418 and DT-A with Southern analysis, then aggregated with single eight-cell embryos from CD-1 mice (Yoshizawa et al., 1997). Chimeric mice were then crossed with a general deleter mouse line, *ACTB-Flpe* (Jackson Laboratory), to remove the *Kan^r/Neo^r* cassette. The *Ctsk-Cre* mice (*Ctsk$^{Cre/+}$*), originally on a hybrid C57BL/6 and CBA genetic background, were backcrossed for four generations into a C57BL/6J background. *FasL$^{gld/gld}$* mice were also purchased from Jackson Laboratory.

Analysis of Cre Recombinase Activities

Expression of the Cre transcript was detected by RT-PCR. Southern analysis using a *Cre* cDNA probe was performed with total RNA extracted from 12-week-old mice. To evaluate the specificity and efficiency of Cre-mediated recombination, we mated the *Ctsk$^{Cre/+}$* mice to *CAG-CAT-Z* reporter mice (kindly provided by J. Miyazaki) (Sakai and Miyazaki, 1997) and genotyped their offspring with *Cre*-specific primers. β-galactosidase activity of the expressed *LacZ* gene driven by the *CAG* promoter was expected to be detected in the given cells expressing functional Cre recombinase.

In Vitro Osteoclastogenesis and Ligand Application

Bone-marrow cells derived from 8-week-old mice were plated in culture dishes containing α-MEM (GIBCO-BRL) with 10% FBS (JRH) and 10 ng/ml M-CSF (Genzyme). After incubation for 48 hr, adherent cells were used as osteoclast precursor cells after washing out the nonadherent cells. Cells were cultured in the presence of 10 ng/ml M-CSF and 100 ng/ml RANKL (Peprotech) to generate osteoclast-like cells (Koga et al., 2004) for 3 days, so the total culture time was 5 days. Three days after RANKL stimulation, primary cultured osteoclasts were treated with 10^{-8} M of 17β-estradiol (E2) (Sigma-Aldrich Co.) or 10^{-6} M 4-hydroxytamoxifen (Tam) (Sigma-Aldrich Co.) in phenol-red free medium.

Generation of Osteoclast-Specific ERα KO Mice

The ERα conditional (*ERα$^{flox/flox}$*) (Dupont et al., 2000) and null alleles with a C57BL/6J background have been previously described. *ERα$^{flox/flox}$* mice were crossed with *Ctsk$^{Cre/+}$* mice to generate *Ctsk$^{Cre/+}$; ERα$^{flox/+}$* mice. *Ctsk$^{Cre/+}$; ERα$^{+/+}$* (*ERα$^{+/+}$*) and *Ctsk$^{Cre/+}$; ERα$^{flox/flox}$* (*ERα$^{ΔOc/ΔOc}$*) mice were obtained by crossing *Ctsk$^{Cre/+}$; ERα$^{flox/+}$* with *ERα$^{flox/+}$* mouse lines.

Radiological Analysis

Bone radiographs of the femurs of 12-week-old *Ctsk$^{Cre/+}$; ERα$^{flox/flox}$* (*ERα$^{ΔOc/ΔOc}$*) and *Ctsk$^{Cre/+}$; ERα$^{+/+}$* (*ERα$^{+/+}$*) littermates were visualized with a soft X-ray apparatus (TRS-1005: SOFTRON). BMD was measured by DXA using a bone mineral analyzer (DCS-600EX: ALOKA). Micro Computed Tomography scanning of the femurs was performed using a composite X-ray analyzer (NX-CP-C80H-IL: Nittetsu ELEX Co.) (Kawano et al., 2003). Tomograms were obtained with a slice thickness of 10 μm and reconstructed at 12 × 12 pixels into a 3D image by the volume-rending method (VIP-Station; Teijin System Technology) using a computer.

Analysis of Skeletal Morphology

Twelve-week-old *Ctsk$^{Cre/+}$; ERα$^{flox/flox}$* (*ERα$^{ΔOc/ΔOc}$*) and *Ctsk$^{Cre/+}$; ERα$^{+/+}$* (*ERα$^{+/+}$*) littermates were double labeled with subcutaneous injections of 16 mg/kg of calcein (Sigma) at 4 and 2 days before sacrifice. Tibiae were removed from each mouse and fixed with 70% ethanol. They were stained with Villanueva bone stain for 7 days and embedded in methyl-methacrylate (Wako) (Yoshizawa et al., 1997). Frontal plane sections (5-μm thick) of the proximal tibia were cut using a Microtome (LEICA). The cancellous bone was measured in the secondary spongiosa located 500 μm from the epiphyseal growth plate and 160 μm from the endocortical surface (Kawano et al., 2003; Nakamichi et al., 2003). Bone histomorphometric measurements of the tibia were made using a semiautomatic image analyzing system (System Supply) and a fluorescent microscope (Optiphot; Nikon). Similar measurements of the lumbar vertebral bodies were done as previously reported (Takeda et al., 2002). Standard bone histomorphometrical nomenclatures, symbols, and units were used as described in the report of the ASBMR Histomophometry Nomenclature Committee.

Ovariectomy and Hormone Replacement

Female *Ctsk$^{Cre/+}$; ERα$^{flox/flox}$* (*ERα$^{ΔOc/ΔOc}$*) and *Ctsk$^{Cre/+}$; ERα$^{+/+}$* (*ERα$^{+/+}$*) littermates were ovariectomized or sham operated at 8–12 weeks of age for 2 weeks for all experiments, and slow releasing pellets of E2 (0.83 μg/day) or placebo (Innovative Research, Sarasota, FL) were implanted subcutaneously in the scapular region behind the neck (Sato et al., 2004; Shiina et al., 2006).

Immunohistochemistry

Twelve-week-old *Ctsk$^{Cre/+}$; ERα$^{flox/flox}$* (*ERα$^{ΔOc/ΔOc}$*) and *Ctsk$^{Cre/+}$; ERα$^{+/+}$* (*ERα$^{+/+}$*) littermates were fixed with 4% PFA by perfusion. Serial sections of the brain (20 μm thick) were divided into two groups and used for single labeling for the ERα or thionin to allow determination of the areas to be measured. Tibiae and femurs were decalcified in 10% EDTA for 2–4 weeks after fixation and then embedded in paraffin sections. Sections were incubated in L.A.B. solution (Polysciences) for 30 min to retrieve antigen. The cooled sections were incubated in 1% H_2O_2 for 30 min to quench endogenous peroxidase and then washed with 1% Triton X-100 in PBS for 10 min. To block nonspecific antibody binding, sections were incubated in blocking solution (DAKO) for 5 min. Sections were then incubated with anti-ERα (Santa Cruz, CA) and anti-FasL (Santa Cruz, CA) in blocking solution overnight at 4°C. Staining was then performed using the EnVision+ HRP System (Dako) and 3, 3′-diaminobendizine tetrahydrochloride substrate (Sigma), counterstained with TRAP, dehydrated through an ethanol series and xylene, before mounting (Sato et al., 2004).

ERα Overexpression

Two days after RANKL stimulation, an expression vector of mouse ERα was tranfected into immature osteoclastic cells from *ERα$^{ΔOc/ΔOc}$* mice using Superfect (QIAGEN) as manufacture's instruction.

Real-Time RT-PCR

One microgram of total RNA from each sample was reverse transcribed into first-strand cDNA with random hexamers using Superscript III reverse transcriptase (Invitrogen). Primer sets for all genes were purchased from Takara Bio. Inc. (Tokyo, Japan). Real-time RT-PCR was performed using SYBR Premix Ex Taq (Takara) with the ABI PRISM 7900HT (Applied Biosystems) according to the manufacturer's instructions. Experimental samples were matched to a standard curve generated by amplifying serially diluted products using the same PCR protocol. To correct for variability in RNA recovery and efficiency of reverse transcription, *Gapdh* cDNA was amplified and quantified in each cDNA preparation. Normalization and calculation steps were performed as reported previously (Takezawa et al., 2007).

TUNEL/TRAP Staining

The TUNEL method was performed using the ApopTag Fluorescein In Situ Apoptosis Detection Kit (CHEMICON international) according to the manufacturer's instructions with a slight modification. This was followed by TRAP staining as previously reported (Kobayashi et al., 2000).

Cytokine Assays

Bone marrow and blood were collected at 2 weeks after sham operation or ovariectomy. Bone-marrow cells were cultured for 3 days in DMEM. The levels of TNFα, IL-1α, and IL-6 in the culture media and serum RANKL were determined by ELISA (R&D Systems).

Western Blot

Osteoclast precursor cells were treated with or without 100 ng/ml of soluble RANKL. After 15 minutes, cell extracts were harvested from the cells using lysis buffer containing 100 mM Tris-HCl (pH 7.8), 150 mM NaCl, 0.1% Triton X-100, 5% protease inhibitor cocktail (Sigma), and 5% phosphatase inhibitor cocktail (Sigma). An equivalent amount of protein from each of the cell extracts and proteins of femoral bone extracted using ISOGEN was loaded for SDS-PAGE and transferred to PVDF membranes (Amersham Biosciences). The membranes were developed with enhanced chemiluminescence reagent (Amersham Biosciences) (Ohtake et al., 2003). Phosphorylation of p38 MAPK and IκB were evaluated using antibodies purchased from Cell Signaling Technology (Koga et al., 2004) and anti-FasL antibody was purchased from Santa Cruz Biotechnology (sc-834).

Actin-Ring Formation

Cells were fixed for 15 min in warm 4% paraformaldehyde (PFA). After fixation, cells were washed three times with PBS with 0.1% Triton X-100 (PBST) and incubated with 0.2 U/ml rhodamine phalloidin (Molecular Probes) for 30 min and washed again three times in PBST.

Statistical Analysis

Data were analyzed by two-tailed student's t test. For all graphs, data are represented as mean ± SEM.

Supplemental Data

Supplemental Data include Supplemental Experimental Procedures and four figures and can be found with this article online at http://www.cell.com/cgi/content/full/130/5/811/DC1/.

ACKNOWLEDGMENTS

We thank Drs. S. Krum and M. Brown to share with their unpublished results; Drs. K. Yoshimura, Y. Nakamichi, T. Watanabe, J. Miyamoto, H. Shiina, T. Fukuda, Ms. Y. Sato, and S. Tanaka for generation of the KO mice; Drs. T. Koga, H. Takagi, E. Ochiai, and N. Moriyama for technical help; Dr. J. Miyazaki for *CAG-CAT-Z* reporter mice, and H. Higuchi and K. Hiraga for manuscript preparation. This work was supported in part by priority areas from the Ministry of Education, Culture, Sports, Science and Technology (to S.K.) and the Program for Promotion of Basic Research Activities for Innovative Biosciences (PROBRAIN).

Received: February 23, 2007
Revised: May 21, 2007
Accepted: July 17, 2007
Published: September 6, 2007

REFERENCES

Belandia, B., and Parker, M.G. (2003). Nuclear receptors: a rendezvous for chromatin remodeling factors. Cell *114*, 277–280.

Bland, R. (2000). Steroid hormone receptor expression and action in bone. Clin. Sci. (Lond.) *98*, 217–240.

Carroll, J.S., Liu, X.S., Brodsky, A.S., Li, W., Meyer, C.A., Szary, A.J., Eeckhoute, J., Shao, W., Hestermann, E.V., Geistlinger, T.R., et al. (2005). Chromosome-wide mapping of estrogen receptor binding reveals long-range regulation requiring the forkhead protein FoxA1. Cell *122*, 33–43.

Chien, K.R., and Karsenty, G. (2005). Longevity and lineages: toward the integrative biology of degenerative diseases in heart, muscle, and bone. Cell *120*, 533–544.

Copeland, N.G., Jenkins, N.A., and Court, D.L. (2001). Recombineering: a powerful new tool for mouse functional genomics. Nat. Rev. Genet. *2*, 769–779.

Couse, J.F., and Korach, K.S. (1999). Estrogen receptor null mice: what have we learned and where will they lead us? Endocr. Rev. *20*, 358–417.

Delmas, P.D. (2002). Treatment of postmenopausal osteoporosis. Lancet *359*, 2018–2026.

Dupont, S., Krust, A., Gansmuller, A., Dierich, A., Chambon, P., and Mark, M. (2000). Effect of single and compound knockouts of estrogen receptors alpha (ERalpha) and beta (ERbeta) on mouse reproductive phenotypes. Development *127*, 4277–4291.

Gowen, M., Lazner, F., Dodds, R., Kapadia, R., Feild, J., Tavaria, M., Bertoncello, I., Drake, F., Zavarselk, S., Tellis, I., et al. (1999). Cathepsin K knockout mice develop osteopetrosis due to a deficit in matrix degradation but not demineralization. J. Bone Miner. Res. *14*, 1654–1663.

Harada, S., and Rodan, G.A. (2003). Control of osteoblast function and regulation of bone mass. Nature *423*, 349–355.

Kameda, T., Mano, H., Yuasa, T., Mori, Y., Miyazawa, K., Shiokawa, M., Nakamaru, Y., Hiroi, E., Hiura, K., Kameda, A., et al. (1997). Estrogen inhibits bone resorption by directly inducing apoptosis of the bone-resorbing osteoclasts. J. Exp. Med. *186*, 489–495.

Karsenty, G. (2006). Convergence between bone and energy homeostases: leptin regulation of bone mass. Cell Metab. *4*, 341–348.

Karsenty, G., and Wagner, E.F. (2002). Reaching a genetic and molecular understanding of skeletal development. Dev. Cell *2*, 389–406.

Kato, S., Ito, S., Noguchi, T., and Naito, H. (1989). Effects of brefeldin A on the synthesis and secretion of egg white proteins in primary cultured oviduct cells of laying Japanese quail (Coturnix coturnix japonica). Biochim. Biophys. Acta *991*, 36–43.

Kawano, H., Sato, T., Yamada, T., Matsumoto, T., Sekine, K., Watanabe, T., Nakamura, T., Fukuda, T., Yoshimura, K., Yoshizawa, T., et al. (2003). Suppressive function of androgen receptor in bone resorption. Proc. Natl. Acad. Sci. USA *100*, 9416–9421.

Kimble, R.B., Matayoshi, A.B., Vannice, J.L., Kung, V.T., Williams, C., and Pacifici, R. (1995). Simultaneous block of interleukin-1 and tumor necrosis factor is required to completely prevent bone loss in the early postovariectomy period. Endocrinology *136*, 3054–3061.

Kobayashi, Y., Hashimoto, F., Miyamoto, H., Kanaoka, K., Miyazaki-Kawashita, Y., Nakashima, T., Shibata, M., Kobayashi, K., Kato, Y., and Sakai, H. (2000). Force-induced osteoclast apoptosis in vivo is accompanied by elevation in transforming growth factor beta and osteoprotegerin expression. J. Bone Miner. Res. *15*, 1924–1934.

Koga, T., Inui, M., Inoue, K., Kim, S., Suematsu, A., Kobayashi, E., Iwata, T., Ohnishi, H., Matozaki, T., Kodama, T., et al. (2004). Costimulatory signals mediated by the ITAM motif cooperate with RANKL for bone homeostasis. Nature *428*, 758–763.

Li, C.Y., Jepsen, K.J., Majeska, R.J., Zhang, J., Ni, R., Gelb, B.D., and Schaffler, M.B. (2006). Mice lacking Cathepsin K maintain bone remodeling but develop bone fragility despite high bone mass. J. Bone Miner. Res. *21*, 865–875.

Mangelsdorf, D.J., Thummel, C., Beato, M., Herrlich, P., Schutz, G., Umesono, K., Blumberg, B., Kastner, P., Mark, M., Chambon, P., and Evans, R.M. (1995). The nuclear receptor superfamily: the second decade. Cell *83*, 835–839.

Martin, T.J., and Sims, N.A. (2005). Osteoclast-derived activity in the coupling of bone formation to resorption. Trends Mol. Med. *11*, 76–81.

Mueller, S.O., and Korach, K.S. (2001). Estrogen receptors and endocrine diseases: lessons from estrogen receptor knockout mice. Curr. Opin. Pharmacol. *1*, 613–619.

Mundy, G.R., and Elefteriou, F. (2006). Boning up on ephrin signaling. Cell *126*, 441–443.

Nakamichi, Y., Shukunami, C., Yamada, T., Aihara, K., Kawano, H., Sato, T., Nishizaki, Y., Yamamoto, Y., Shindo, M., Yoshimura, K., et al. (2003). Chondromodulin I is a bone remodeling factor. Mol. Cell. Biol. *23*, 636–644.

Ohtake, F., Takeyama, K., Matsumoto, T., Kitagawa, H., Yamamoto, Y., Nohara, K., Tohyama, C., Krust, A., Mimura, J., Chambon, P., et al. (2003). Modulation of oestrogen receptor signalling by association with the activated dioxin receptor. Nature *423*, 545–550.

Raisz, L.G. (2005). Pathogenesis of osteoporosis: concepts, conflicts, and prospects. J. Clin. Invest. *115*, 3318–3325.

Riggs, B.L., and Hartmann, L.C. (2003). Selective estrogen-receptor modulators–mechanisms of action and application to clinical practice. N. Engl. J. Med. *348*, 618–629.

Rodan, G.A., and Martin, T.J. (2000). Therapeutic approaches to bone diseases. Science *289*, 1508–1514.

Saftig, P., Hunziker, E., Wehmeyer, O., Jones, S., Boyde, A., Rommerskirch, W., Moritz, J.D., Schu, P., and von Figura, K. (1998). Impaired osteoclastic bone resorption leads to osteopetrosis in Cathepsin-K-deficient mice. Proc. Natl. Acad. Sci. USA *95*, 13453–13458.

Sakai, K., and Miyazaki, J. (1997). A transgenic mouse line that retains Cre recombinase activity in mature oocytes irrespective of the cre transgene transmission. Biochem. Biophys. Res. Commun. *237*, 318–324.

Sato, T., Matsumoto, T., Kawano, H., Watanabe, T., Uematsu, Y., Sekine, K., Fukuda, T., Aihara, K., Krust, A., Yamada, T., et al. (2004). Brain masculinization requires androgen receptor function. Proc. Natl. Acad. Sci. USA *101*, 1673–1678.

Shang, Y., and Brown, M. (2002). Molecular determinants for the tissue specificity of SERMs. Science *295*, 2465–2468.

Shiina, H., Matsumoto, T., Sato, T., Igarashi, K., Miyamoto, J., Takemasa, S., Sakari, M., Takada, I., Nakamura, T., Metzger, D., et al. (2006). Premature ovarian failure in androgen receptor-deficient mice. Proc. Natl. Acad. Sci. USA *103*, 224–229.

Simpson, E.R., and Davis, S.R. (2001). Minireview: aromatase and the regulation of estrogen biosynthesis–some new perspectives. Endocrinology *142*, 4589–4594.

Sims, N.A., Clement-Lacroix, P., Minet, D., Fraslon-Vanhulle, C., Gaillard-Kelly, M., Resche-Rigon, M., and Baron, R. (2003). A functional androgen receptor is not sufficient to allow estradiol to protect bone after gonadectomy in estradiol receptor-deficient mice. J. Clin. Invest. *111*, 1319–1327.

Smith, E.P., Boyd, J., Frank, G.R., Takahashi, H., Cohen, R.M., Specker, B., Williams, T.C., Lubahn, D.B., and Korach, K.S. (1994). Estrogen resistance caused by a mutation in the estrogen-receptor gene in a man. N. Engl. J. Med. *331*, 1056–1061.

Sun, L., Peng, Y., Sharrow, A.C., Iqbal, J., Zhang, Z., Papachristou, D.J., Zaidi, S., Zhu, L.L., Yaroslavskiy, B.B., Zhou, H., et al. (2006). FSH directly regulates bone mass. Cell *125*, 247–260.

Suzawa, M., Takada, I., Yanagisawa, J., Ohtake, F., Ogawa, S., Yamauchi, T., Kadowaki, T., Takeuchi, Y., Shibuya, H., Gotoh, Y., et al. (2003). Cytokines suppress adipogenesis and PPAR-gamma function through the TAK1/TAB1/NIK cascade. Nat. Cell Biol. *5*, 224–230.

Syed, F., and Khosla, S. (2005). Mechanisms of sex steroid effects on bone. Biochem. Biophys. Res. Commun. *328*, 688–696.

Takeda, S., Elefteriou, F., Levasseur, R., Liu, X., Zhao, L., Parker, K.L., Armstrong, D., Ducy, P., and Karsenty, G. (2002). Leptin regulates bone formation via the sympathetic nervous system. Cell *111*, 305–317.

Takezawa, S., Yokoyama, A., Okada, M., Fujiki, R., Iriyama, A., Yanagi, Y., Ito, H., Takada, I., Kishimoto, M., Miyajima, A., et al. (2007). A cell cycle-dependent co-repressor mediates photoreceptor cell-specific nuclear receptor function. EMBO J. *26*, 764–774.

Teitelbaum, S.L. (2006). Osteoclasts; culprits in inflammatory osteolysis. Arthritis Res. Ther. *8*, 201.

Teitelbaum, S.L. (2007). Osteoclasts: what do they do and how do they do it? Am. J. Pathol. *170*, 427–435.

Teitelbaum, S.L., and Ross, F.P. (2003). Genetic regulation of osteoclast development and function. Nat. Rev. Genet. *4*, 638–649.

Tolar, J., Teitelbaum, S.L., and Orchard, P.J. (2004). Osteopetrosis. N. Engl. J. Med. *351*, 2839–2849.

Windahl, S.H., Andersson, G., and Gustafsson, J.A. (2002). Elucidation of estrogen receptor function in bone with the use of mouse models. Trends Endocrinol. Metab. *13*, 195–200.

Yoshizawa, T., Handa, Y., Uematsu, Y., Takeda, S., Sekine, K., Yoshihara, Y., Kawakami, T., Arioka, K., Sato, H., Uchiyama, Y., et al. (1997). Mice lacking the vitamin D receptor exhibit impaired bone formation, uterine hypoplasia and growth retardation after weaning. Nat. Genet. *16*, 391–396.

Zaman, G., Jessop, H.L., Muzylak, M., De Souza, R.L., Pitsillides, A.A., Price, J.S., and Lanyon, L.L. (2006). Osteocytes use estrogen receptor alpha to respond to strain but their ERalpha content is regulated by estrogen. J. Bone Miner. Res. *21*, 1297–1306.

Accession Numbers

Microarray can be seen in Gene Expression Omnibus under accession number GSE7798.

ELSEVIER

Bone 40 (2007) 876–887

BONE

www.elsevier.com/locate/bone

Effects of aromatase inhibitors on human osteoblast and osteoblast-like cells: A possible androgenic bone protective effects induced by exemestane

Yasuhiro Miki [a], Takashi Suzuki [a], Masahito Hatori [b], Katsuhide Igarashi [c], Ken-ich Aisaki [c], Jun Kanno [c], Yasuhiro Nakamura [a], Miwa Uzuki [d], Takashi Sawai [c], Hironobu Sasano [a,*]

[a] *Department of Pathology, Tohoku University Graduate School of Medicine, 2-1 Seiryo-machi, Aoba-ku, Sendai, Miyagi, 980-8575, Japan*
[b] *Department of Orthopedic Surgery, Tohoku University Graduate School of Medicine, Sendai, Japan*
[c] *Division of Toxicology, National Institute of Health Sciences, Biological Safety Research Center, Setagaya, Tokyo, Japan*
[d] *Department of Pathology, Iwate Medical College, Morioka, Japan*

Received 21 April 2006; revised 6 November 2006; accepted 14 November 2006
Available online 28 December 2006

Abstract

Effects of aromatase inhibitors (AIs) on the human skeletal system due to systemic estrogen depletion are becoming clinically important due to their increasing use as an adjuvant therapy in postmenopausal women with breast cancer. However, possible effects of AIs on human bone cells have remained largely unknown. We therefore studied effects of AIs including the steroidal AI, exemestane (EXE), and non-steroidal AIs, Aromatase Inhibitor I (AI-I) and aminoglutethimide (AGM), on a human osteoblast. We employed a human osteoblast cell line, hFOB, which maintains relatively physiological status of estrogen and androgen pathways of human osteoblasts, i.e., expression of aromatase, androgen receptor (AR), and estrogen receptor (ER) β. We also employed osteoblast-like cell lines, Saos-2 and MG-63 which expressed aromatase, AR, and ERα/β in order to further evaluate the mechanisms of effects of AIs on osteoblasts. There was a significant increment in the number of the cells following 72 h treatment with EXE in hFOB and Saos-2 but not in MG-63, in which the level of AR mRNA was lower than that in hFOB and Saos-2. Alkaline phosphatase activity was also increased by EXE treatment in hFOB and Saos-2. Pretreatment with the AR blocker, flutamide, partially inhibited the effect of EXE. AI-I exerted no effects on osteoblast cell proliferation and AGM diminished the number of the cells. hFOB converted androstenedione into E2 and testosterone (TST). Both EXE and AI-I decreased E2 level and increased TST level. In a microarray analysis, gene profile patterns following treatment with EXE demonstrated similar patterns as with DHT but not with E2 treatment. The genes induced by EXE treatment were related to cell proliferation, differentiation which includes genes encoding cytoskeleton proteins. We also examined the expression levels of these genes using quantitative RT-PCR in hFOB and Saos-2 treated with EXE and DHT and with/without flutamide. HOXD11 gene known as bone morphogenesis factor and osteoblast growth-related genes were induced by EXE treatment as well as DHT treatment in both hFOB and Saos-2. These results indicated that the steroidal aromatase inhibitor, EXE, stimulated hFOB cell proliferation via both AR dependent and independent pathways.

Keywords: Osteoblast; Aromatase inhibitor; Androgen; Estrogen; Exemestane

Introduction

Results in various epidemiological or clinical studies demonstrated that estrogens play important protective roles in human skeletal as well as cardiovascular systems, and estrogen deficiency resulted in accelerating the development of osteoporosis in postmenopausal women [1–3]. In breast cancer of postmenopausal women, hormone therapies without any clinically deleterious effects due to estrogen deficiency on bone metabolism as well as lipid metabolisms are preferable. Estrogen deficiency has been generally detected in the patients with breast cancer following chemotherapy induced ovarian failure, gonadotropin analogue, and aromatase inhibitors (AIs) therapy [4]. Aromatase is the pivotal enzyme of *in situ* or intratumoral estrogen biosynthesis in postmenopausal breast cancer patients, and catalyzes the conversion from androgens into estrogens (Fig. 1A). AIs therefore play an important role in

* Corresponding author. Fax: +81 22 273 5976.
E-mail address: hsasano@patholo2.med.tohoku.ac.jp (H. Sasano).

8756-3282/$ - see front matter © 2006 Elsevier Inc. All rights reserved.
doi:10.1016/j.bone.2006.11.029

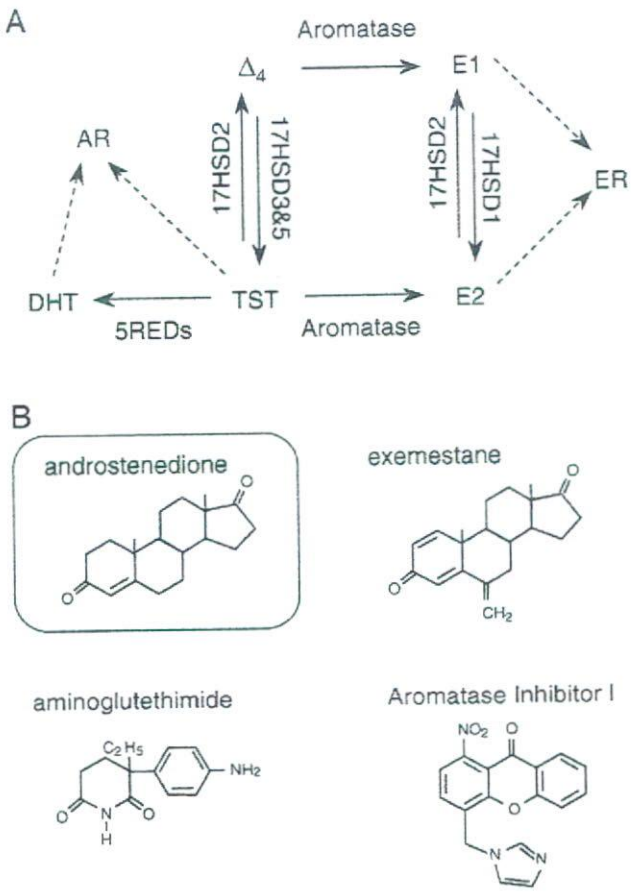

Fig. 1. (A) Summary of the pathway of estrogens and androgens production. Aromatase catalyzes the change from androstenedione (Δ4) and testosterone (TST) into estrone (E1) and estradiol (E2), respectively. 17HSD, 17β-hydroxysteroid dehydrogenase; 5REDs, 5α-reductase types 1 and 2; AR, androgen receptor; DHT, 5α-dihydrotestosterone; ER, estrogen receptor. (B) Structure of aromatase inhibitors used in this study. Androstenedione is a natural substrate of aromatase. Steroidal aromatase inhibitor, exemestane has an androstenedione-like structure.

clinical management of both primary and advanced breast cancer in postmenopausal women [5]. AIs are classified into two classes according to their modes of action. Type I AIs are steroidal inhibitions and one of them, exemestane (EXE) inhibits aromatase irreversibly and has an androstenedione (Δ_4)-like structure (Fig. 1B) [5–7]. Type II AIs are non-steroidal inhibitions and include aminoglutethimide (AGM), anastrozole, and letrozole [5].

Results of *in vivo* study using ovariectomized (OVX) rats demonstrated that EXE and its principal metabolite form, 17-hydroexemestane (17H-EXE) but not letrozole significantly prevented bone loss in OVX rats [8,9]. EXE and its principal metabolite, 17H-EXE, are structurally related to Δ_4 and bind to androgen receptor (AR) with relatively low affinity compared to 5α-dihydrotestosterone (DHT) [7]. These finding suggest that EXE may demonstrate protective effects toward bone tissues through its androgenic actions. However, detailed mechanisms of effects of EXE or androgen itself on human bone cells have remained largely unknown.

Various studies using human or animal bone tissues [10,11] and osteoblast cell culture using osteosarcoma cells [12,13] demonstrated that aromatase mRNA or protein was detected in osteoblast cells, which play an important role in bone remodeling. Therefore, in this study, we focused on effects of EXE in human osteoblast in an initial attempt to evaluate the effects of these AIs (summarized in Table 1 and Fig. 1B) [5–7,14], including AGM, EXE, and an experimental compound for inhibition of aromatase, Aromatase Inhibitor I (AI-I) [14] on human osteoblast and osteoblast-like cell lines. In our present study, we employed normal human cell line, hFOB, which maintains native characteristics of sex steroid hormone pathway of human osteoblasts, i.e., expression of AR, ERβ but not ERα, and aromatase. We also employed other osteoblast-like cell lines, Saos-2 and MG-63 which expressed ERα as well as ERβ in order to further study the mechanisms of effects of AI on human osteoblasts. We first examined the effects of estradiol (E2), DHT, progesterone (Prg), and AIs described above on cell proliferation of these cell lines, because the status of cell proliferation is important in the maintenance of homeostasis of bone tissue [15]. In addition, the effects of AIs on the conversion ratio of Δ_4 into E2 or testosterone (TST) in hFOB cultured medium were examined. We then screened E2, DHT, and EXE responsive genes using a microarray analysis in these cells, in order to further characterize the possible genomic effects of EXE on cell proliferation of osteoblasts. In this microarray analysis, hFOB was employed in order to examine the effects of E2, DHT, and EXE on native status of human osteoblasts but not on pathological status of osteoblasts such as osteosarcomas.

Materials and methods

Chemicals

Exemestane (EXE; FCE24304; 6-methyleneandrosta-1,4-diene-3,17-dione and 17-hydroexemestane (17H-EXE; FCE25071; 6-methyleneandrosta-1,4-diene-17β-ol-3-one) were obtained from Pfizer, Inc. (MI, USA). Aminoglutethimide (AGM) and Aromatase Inhibitor I [AI-I; 4-(Imidazolylmethyl)-1-nitro-9*H*-9-xanthenone] were obtained from Sigma-Aldrich Co. (MO, USA) and EMD Biosciences, Inc. (CA, USA), respectively. Estradiol (E2), progesterone (Prg), and RU38,486 (RU; mifepristone), spironolactone were obtained from Sigma-Aldrich. ICI 182,780 (ICI; fulvestrant) and hydroxyflutamide (OHF) were obtained from Tocris Cookson Inc. (MO, USA) and Toronto Research Chemicals, Inc. (Ontario, Canada), respectively. 5α-dihydrotestosterone (DHT) was obtained from Wako Pure Chemical industries, Ltd. (Osaka, Japan).

Table 1
Aromatase inhibitors used in this study

	Aminoglutethimide	Exemestane	Aromatase inhibitor
Trademark[a]	Cytadren®	Aromasin®	–
Type[b]	Type II	Type I	Type II
Generation	First	Third	–
IC50 (nM)[c]	3000	50	40

[a] Cytadren® is trademark of Novartis Pharmaseutical Corporation. Aromasin is trademark of Pfizer Inc. Aromatase Inhibitor I is non-clinical compound c Calbiochem®.

[b] Type I is steroidal compound. Type II is a non-steroidal compound.

[c] Refs, Aminoglutethimide and Exemestane are Miller et al. [5]; Aromatase Inhibitor I is Recanatini et al. [14].

These materials were dissolved in pure ethanol (Wako Pure Chemical industries) and serially diluted (final concentrations: 10^{-12} M to 10^{-5} M), respectively. AGM was dissolved in DMSO (Wako Pure Chemical industries). The final concentration of ethanol and DMSO used in this study did not exceed 0.05%.

Osteoblast cell and osteoblast-like cell lines and culture conditions

Human normal osteoblast cell, hFOB 1.19 cell line (CRL-11372) was obtained from American Type Culture Collection (VA, USA). hFOB 1.19 cell was cultured according to the protocol previously described [16]. The cell line was maintained in a mixture of Dulbecco's Modified Eagle Medium and Ham's F12 medium (1:1) without phenol red (Invitrogen Corporation, CA, USA) supplemented with 10% fetal bovine serum (FBS; JRH Biosciences, KS, USA) and 50 mg/mL G 418 sulfate (EMD Biosciences). Human osteosarcoma cell lines Saos-2 and MG-63 were provided from the Cell Resource Center for Biomedical Research, Tohoku University (Sendai, Japan) and were maintained in a RPMI-1640 (Sigma-Aldrich) with 10% FBS. These cells were pre-incubated for 24 h with FBS-free medium prior to examination in order to remove exo-/endogenous steroid hormones from the culture medium and study the effects of various compounds in the absence of steroids and also to synchronize the cell cycle. Different concentrations of test compounds were added, and the assay was terminated after 3 or 5 days by removing the medium from wells. Steroid blockers were added simultaneously.

Characteristics of hFOB, Saos-2, and MG-63

Expressions of relevant steroid receptors, i.e., ERα, ERβ, and AR were determined using quantitative RT-PCR methods in hFOB, Saos-2, and MG-63 cell lines. mRNA transcripts of steroid synthesis/metabolite enzymes, aromatase, 17β-hydroxysteroid dehydrogenase (17β-HSD) types 1, 2, 3, 4, and 5, and 5α-reductase (5α-Red) types 1 and 2 were all evaluated using RT-PCR methods. The details of quantitative RT-PCR including primer sets employed were previously described in detail [17,18]. Positive controls for these receptors and enzymes were cell lines of human breast cancer, T-47D, and human prostate cancer, LNCaP obtained from Cell Resource Center for Biomedical Research, Tohoku University (Sendai, Japan). Alkaline phosphatase (ALP), an osteoblast-specific marker, was also studied using RT-PCR for characterization of these cell lines.

Estradiol and testosterone production assay

hFOB cells were plated in 10 mm dishes at a density of 10^6 viable cells and cultured for 48 h. Then media were changed to FBS-free medium, and hFOB cells were incubated with 10^{-7} M androstenedione (Δ_4; Sigma-Aldrich) in the presence or absence of EXE or AI-I (10^{-7} M). The media were then collected after 24 h, and E2 and TST were measured by solid-phase radioimmunoassay. Radioimmunoassay was performed in SRL Inc. (Tokyo, Japan) using DPC estradiol kit and DPC total testosterone kit (Diagnostic Products Corporation, LA, USA). In addition, we confirmed that the concentrations of E2 and TST were under the detection limits (E2, 5 pg/mL; TST, 30 pg/mL) in the serum- and phenol red-free medium.

Cell proliferation assay

hFOB, Saos-2, and MG-63 cells were treated with steroids and test compounds for 24, 48, and 72 h, when specimens were harvested and evaluated for cell proliferation using the WST-8 method (Cell Counting Kit-8; Dojindo Inc., Kumamoto, Japan) [18]. Optical densities (OD, 450 nm) were evaluated using a SpectraMax 190 microplate reader (Molecular Devices, Corp., CA, USA) and Softmax Pro 4.3 microplate analysis software (Molecular Devices). The status of proliferation (%) was calculated according to the following equation: (cell OD value after test materials treated/vehicle control cell OD value) × 100.

Alkaline phosphatase activity assay

hFOB, Saos-2, and MG-63 cells were plated in 48 well plate at a density of 10^6 viable cells and cultured for 48 h. All cell lines were treated with 10^{-9} to 10^{-7} M exemestane for 72 h, when cells were lysed with 0.05% Triton X-100 (Wako Pure Chemical industries) and evaluated for alkaline phosphatase activity

Table 2
Primer sequences used in quantitative RT-PCR analysis

cDNA	GB#	Sequence	cDNA position	Size (bp)
MYBL2	NM_002466	Forward 5′-GTAACAGCCTCACGCCCAAGA-3′ Reverse 5′-TCCAATGTGTCCTGTTTGTTCCA-3′	1522–1615	94
OSTM1	NM_014028	Forward 5′-TTGAGAATAAGGCTGAACCTGGAAC-3′ Reverse 5′-TTACAGGCACTGTGTCACTGCAAG-3′	801–926	126
HOXD11[a]	NM_021192	Forward 5′-CAC TGT CCT TGG GTT TAA TG-3′ Reverse 5′-GGT AAA ATT GTA ACG GGA CG-3′	1091–1245	174
GPC2	NM_152742	Forward 5′-AGA AAT GTG GTC AGC GAA GC-3′ Reverse 5′-ACA CCT TCG CAC TGT TTT CC-3′	871-1183	313
ADCYAP1R1	NM_001118	Forward 5′-CAG CAA AAG GGA AAG ACT CG-3′ Reverse 5′-GAG CTG CTC TTG CTC AGG AT-3′	1351–1584	234
COL1A1	NM_000088	Forward 5′-GGT GGT GGT TAT GAC TTT GGT T-3′ Reverse 5′-CTT GGC TGG GAT GTT TTC AGG T-3′	3784–4092	309
SMAD1[a]	NM_005900	Forward 5′-GGT TCA CCT CAT AAT CCT-3′ Reverse 5′-CCT TTG TCA GTT CTC AAT C-3′	1779–1887	127
SMAD5[a]	NM_005903	Forward 5′-AGC TAA AGC CGT TGG ATA-3′ Reverse 5′-AGG CAC TAA TAC TGG AGG T-3′	668–768	119
RUNX2	NM_004348	Forward 5′-GTG GAC GAG GCA AGA GTT T-3′ Reverse 5′-TAC TGG GAT GAG GAA TGC G-3′	782–961	198
SPARC	NM_003118	Forward 5′-CCT GTA CAC TGG CAG TTC-3′ Reverse 5′-CCA GGG CGA TGT ACT TGT C-3′	793–937	163
ALP	NM_000478	Forward 5′-ACC ATT CCC ACG TCT TCA CA-3′ Reverse 5′-AGA CAT TCT CTC GTT CAC CGC C-3′	1379–1540	162
RPL13A	NM_012423	Forward 5′-CCT GGA GGA GAA GAG GAA AGA GA-3′ Reverse 5′-TTG AGG ACC TCT GTG TAT TTG TCA A-3′	487–612	126

GB#, GeneBank accession number.
All primer sets were designed using OLIGO Primer Analysis Software (TAKARA Bio Inc., Shiga, Japan).
[a] Forward and reverse primers were located in sama exon.

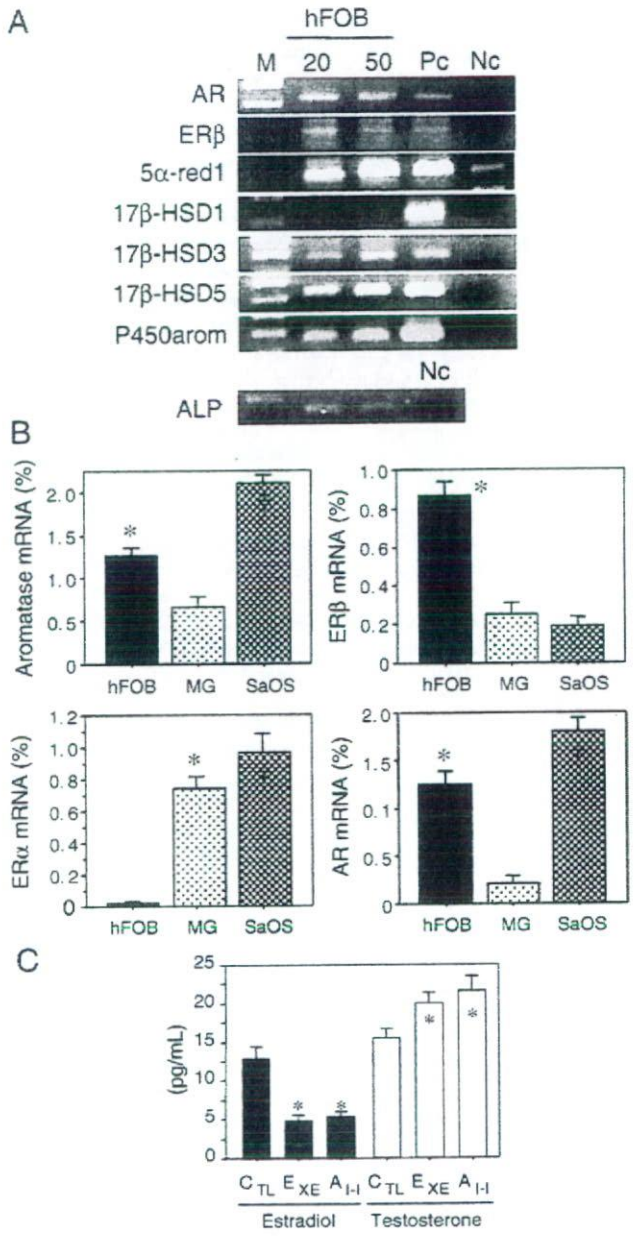

Fig. 2. (A) Results of RT-PCR analysis of steroid hormone receptors and steroid-related enzymes. Both 20 and 50 ng/μL cDNA of hFOB were used for PCR (ALP was 20 ng/μL alone). AR, androgen receptor; ER, estrogen receptor; 5α-red1, 5α-reductase type 1; 17β-HSD, 17β-hydroxysteroid dehydrogenase; P450 arom, aromatase; M, molecular marker; Pc, positive control; Nc, negative control. (B) Expression levels of aromatase, AR, ERα, and ERβ in hFOB, Saos-2, and MG-63. $^{*}p<0.05$ vs. MG-63 (aromatase and AR), vs. MG-63 and vs. Saos-2 (ERβ), vs. hFOB (ERα); $^{\dagger}p<0.05$ vs. hFOB and MG-63 (aromatase and AR), vs. MG-63 and hFOB (ERα). (C) Estradiol and testosterone productions in hFOB cells. The data are expressed as the mean SD ($n=3$). $^{*}p<0.05$ vs. control cells (CTL). EXE, 10^{-7} M exemestane; AI-I, 10^{-7} M aromatase inhibitor I.

using the *p*-nitrophenylphosphate method (LabAssay ALP; Wako Pure Chemical industries) [19]. Optical densities (OD, 405 nm) were evaluated using a SpectraMax 190 microplate reader (Molecular Devices) and Softmax Pro 4.3 microplate analysis software (Molecular Devices). ALP activity (units/μL)=(concentration of *p*-nitrophenol/15 min)×1 (dilution factor of sample). The ALP activities were presented as units/μL/10^6 cells. The ALP activity levels in each case were represented as a ratio of vehicle control (%).

Microarray analysis

The procedure was based on a previously reported study [20]. Cell lysates were prepared using RLT buffer (QIAGEN GmbH, Hilden, Germany). Total RNA was extracted using RNeasy Mini Kit (QIAGEN). First-strand cDNA was synthesized by incubating 5 μg of total RNA with 200 U SuperScript II reverse transcriptase (Invitrogen), 100 pmol T7-(dT)24 primer (Invitrogen). Ten units of T4 DNA polymerase (Invitrogen) were then added, and the dsDNA was mixed with T7 RNA polymerase (Invitrogen). The purified cRNA was fragmented at 300–500 bp as target solution. Hybridization was performed with the GeneChip Human Genome 133 ver. 2.0 (Affymetrix, Inc., CA, USA). The reacted arrays were then scanned as digital image files and scanned data were analyzed with GeneChip software (Affymetrix). Relative levels of gene expression were calculated by global normalization.

Data were subjected to hierarchical clustering analysis and visualization using the Cluster and TreeView programs (Stanford University) in order to generate tree structures based on the degree of similarity, as well as matrices comparing the levels of expression of individual genes in each sample [21].

Real-time PCR

Real-time PCR was carried out using the LightCycler System and the FastStart DNA Master SYBR Green I (Roche Diagnostics GmbH, Mannheim, Germany). The primer sequences used in this study are summarized in Table 2. An initial denaturing step of 95 °C for 10 min was followed by 35 cycles, respectively, at 95 °C for 10 min; 15 s annealing at 65 °C (ALP, COL1A1), 64 °C (MYBL2, OSTM1, RPL13A), 62 °C (SMAD1, SMAD5, SPARC, RUNX2), or 60 °C (HOXD11); and extension for 15 s at 72 °C. Negative control experiments included those lacking cDNA substrates to confirm the presence of exogenous contaminant DNA. No amplified products were detected under these conditions. The mRNA levels in each case were represented as a ratio of RPL13A (%) [22].

Immunohistochemistry of AR

Five non-pathological bone tissues were retrieved from surgical pathology files (two females and three males, 17 to 55 years old) of Department of Pathology, Tohoku University Hospital (Sendai, Japan).

Tissue sections were immunostained using a biotin-streptavidin method with Histofine kit (Nichirei Co. Ltd., Tokyo, Japan). The monoclonal antibody for AR (AR411) [23] was obtained from DakoCytomation (Kyoto, Japan). Experimental procedures employed in our present study have been previously described in detail [22,23]. The dilutions of primary AR antibody were 1:100. The antigen-antibody complex was then visualized with 3,3′-diaminobenzidine solution, and counterstained with hematoxylin. Prostate cancer was used as a positive control for AR. Normal mouse IgG was used as a negative control for immunostaining and no specific immunoreactivity was detected.

Statistical analysis

Results were expressed as mean±SD. Statistical analysis was performed with the StatView 5.0 J software (SAS Institute Inc., NC, USA). All data were analyzed by analysis of variance (ANOVA) followed by post hoc Bonferroni/Dunnett multiple comparison test. A p-value<0.05 was considered to indicate statistical significance.

Results

Characteristics of hFOB, MG-63, and Saos-2 cell line

Characteristics of osteoblast and osteoblast-like cell lines are summarized in Figs. 2A and B. hFOB cells expressed mRNA transcripts of AR and ERβ. Relatively low level of ERα mRNA transcript was detected in hFOB cells. Aromatase, 17β-HSD type 1, 3, and 5, and 5α-Red types 1 and 2 mRNA transcripts were all detected in hFOB cells by

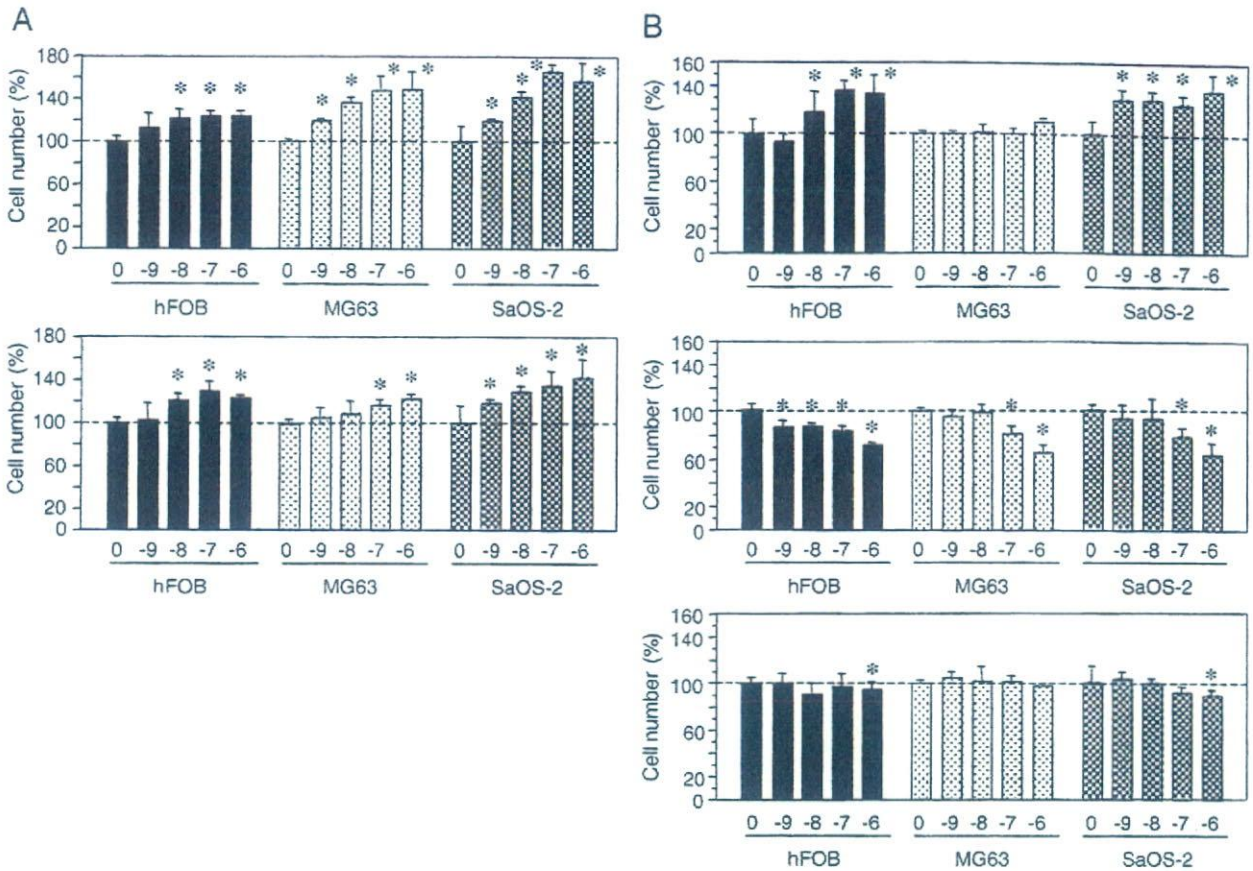

Fig. 3. (A) Proliferation of hFOB cells treated by estradiol (top) and 5α-DHT (bottom). *$p<0.05$ vs. vehicle control (0). (B) Proliferation of hFOB cells treated by exemestane (top), aminogluthetimide (middle), and Aromatase Inhibitor-I (bottom). *$p<0.05$ vs. vehicle control (0). $n=5$.

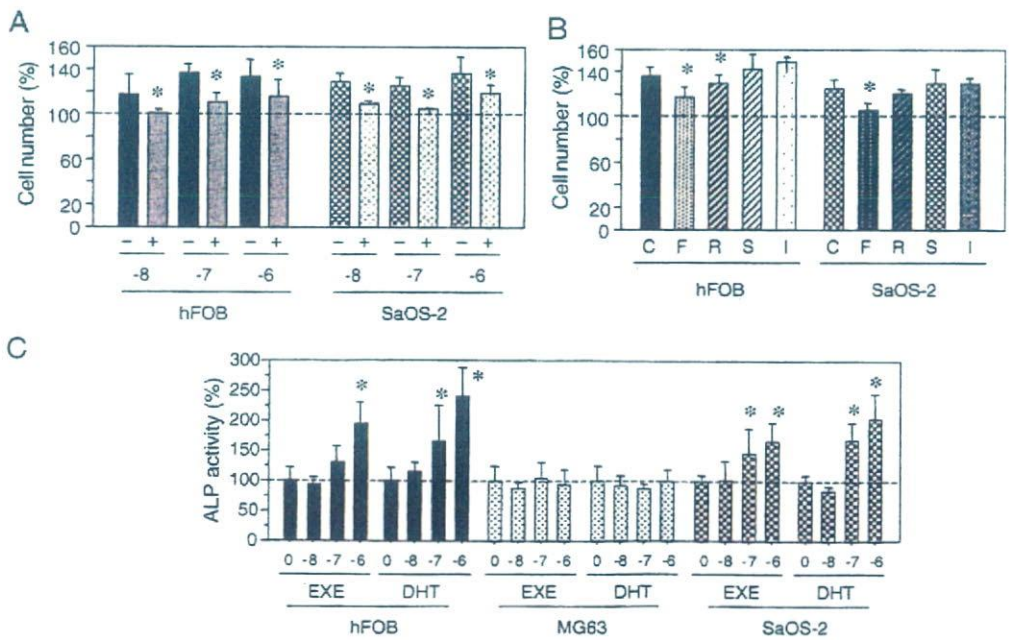

Fig. 4. (A) Effects of hydroxyflutamide on exemestane (10^{-8} to 10^{-6} M) stimulated the cell proliferation of both hFOB and Saos-2. With (+) or without (−) hydroxyflutamide, $p<0.05$ vs. without hydroxyflutamide (*). (B) Effects of steroid receptor blockers on exemestane (10^{-7} M) stimulated cell proliferation of hFOB and Saos-2. C, 10^{-7} M exemestane; F, hydroxyflutamide (5×10^{-6} M); R, RU38,486 (5×10^{-6} M); S, spironolactone (5×10^{-6} M); I, ICI182,720 (5×10^{-6} M). *$p<0.05$ vs. C (C) ALP activity in hFOB, Saos-2, MG-63 treated with exemestane (EXE, 10^{-8} to 10^{-6} M), or 5α-DHT (DHT, 10^{-8} to 10^{-6} M). *$p<0.05$ vs. vehicle control (0).

RT-PCR. Aromatase, ERα, ERβ, and AR were all detected in osteoblast-like cell lines, Saos-2 and MG-63 (Fig. 2B). In hFOB cell, expression of ERβ mRNA was more predominant than that of ERα mRNA. ERα mRNA as well as ERβ mRNA was detected in Saos-2 and MG-63 cells. The levels of AR mRNA expression in both hFOB and Saos-2 were significantly higher ($p=0.01$) than that in MG-63. ALP mRNA was also detected in intact hFOB, Saos-2, and MG-63 cells (data not present), respectively.

Estradiol and testosterone production

Results were summarized in Fig. 2C. The E2 levels in the medium of hFOB supplemented with Δ_4 treated with EXE or AI-I were significantly lower than that of cells without AIs. The levels of TST in the medium of hFOB supplemented with Δ4 treated with EXE or AI-I were significantly higher than that of cells without AIs.

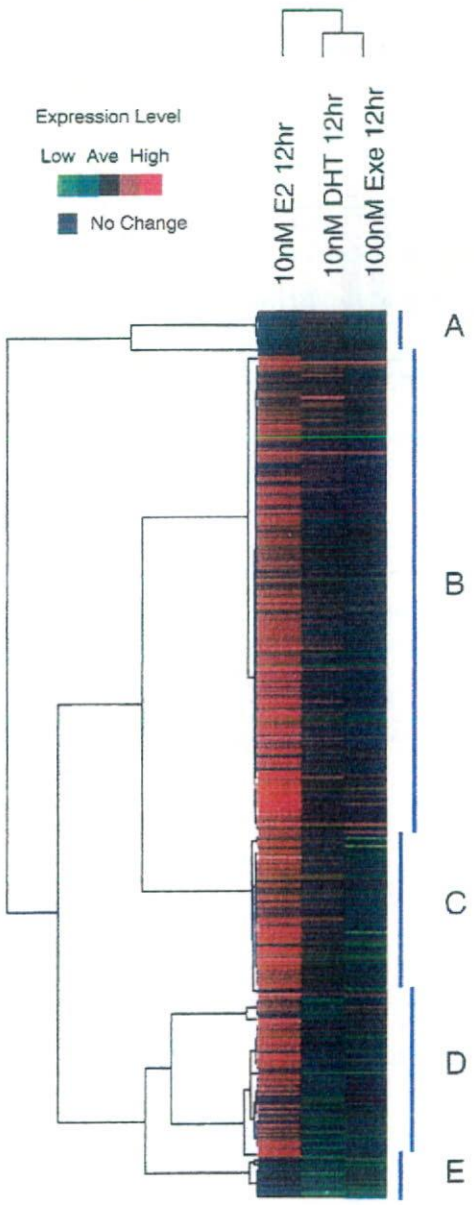

Fig. 5. In clustering analysis of the expression levels of each gene in hFOB cells treated with estradiol (E2), 5α-dihydrotestosterone (DHT), and exemestane (Exe).

Cell proliferation

Results of the cell proliferation assays are summarized in Figs. 3 and 4. There was a significant increment in the number of the cells after 72 h in hFOB, Saos-2, and MG-63 cells treated with 10^{-9} M (Saos-2 and MG-63) or 10^{-8} M (hFOB) to 10^{-6} M E2 (Fig. 3A). The cell number of hFOB and Saos-2 cells treated by 10^{-9} M (Saos-2) or 10^{-8} M (hFOB) to 10^{-6} DHT for 72 h was also significantly higher than control (Fig. 3A). The number of MG-63 cells was significantly increased only by high dose of DHT (10^{-7} M and 10^{-6} M) treatments (Fig. 3A). Prg (10^{-9} M to 10^{-6} M) treatments did not change the number of cells even after 72 h in all three cell lines examined (data not present).

Both EXE (Fig. 3B) and 17H-EXE (data not present) treatments of 10^{-8} M to 10^{-6} M, which were comparable to pharmacological inhibition doses of aromatization (Table 1), significantly increased the hFOB cell number for 72 h, respectively. In Saos-2 cells treated with relatively low dose, 10^{-9} to 10^{-6} M EXE, there was a significant increment in the number of the cells after 72 h (Fig. 3B). However, all the dose (10^{-9} M to 10^{-6} M) of EXE employed did not results in the change of cell number of MG-63 even after 72 h of treatment (Fig. 3B). The cell number of both hFOB and Saos-2 cells treated by both 10^{-6} M EXE and/or 17H-EXE for 48 h was also significantly higher than that treated for 24 h (data not present).

AGM treatment [10^{-9} (hFOB) or 10^{-7} (Saos-2 and MG-63) to 10^{-6} M] diminished the number of these three cells (Fig. 3B) and morphological changes in these cells were consistent with those caused by cytotoxic effects (data not present). AI-I treatment (10^{-9} to 10^{-7} M) was not associated with significant increment of the cell number in these cell lines (Fig. 3B). Only high dose (10^{-6} M) of AI-I significantly diminished the cell numbers of hFOB and Saos-2 but not of MG-63 (Fig. 3B).

The androgen receptor antagonist OHF (5×10^{-6} M) diminished the effects of EXE on these increments of both hFOB and Saos-2 cells (Figs. 4A and B). Treatment with RU but not spironolactone and ICI also inhibited EXE effects on hFOB cells (Fig. 4B).

ALP activity assay

Results of the ALP activity assay were summarized in Fig. 4C. There was a significant increment in the ALP activity of both hFOB and Saos-2 cells treated with 10^{-7} M (Saos-2) and/or 10^{-6} M (hFOB and Saos-2) EXE. Both 10^{-7} M and 10^{-6} M DHT treatment also increased the ALP activity in hFOB and Saos-2 cells, respectively. There were no changes of ALP activity in MG-63 treated with 10^{-8} M to 10^{-6} M of EXE and DHT, respectively.

Table 3a
Genes induced by exemestane treatment in hFOB cells—2.0 higher

	Gene title	Gene symbol	Raw data			Ratio	
			C	D	Ex	D	Ex
NM_002466	V-myb myeloblastosis viral oncogene homolog (avian)-like 2	**MYBL2**	70.9	156.9	150.3	2.2	2.1
AW444985	–	–	57.8	124.7	127.1	2.2	2.2
AF143684	Myosin IXB	MYO9B	48.3	64.4	122.2	1.3	2.5
NM_024682	TBC1 domain family, member 17	TBC1D17	31.7	37.6	64.8	1.2	2.0
BE965311	Chromosome 16 open reading frame 23	C16orf23	29.2	44.2	64.0	1.5	2.2
NM_004233	CD83 antigen (activated B lymphocytes, immunoglobulin superfamily)	CD83	29.0	66.5	60.9	2.3	2.1
AI806031	Skeletal muscle and kidney enriched inositol phosphatase	SKIP	27.7	48.6	55.4	1.8	2.0
AL136729	Ring finger protein 123	RNF123	20.0	23.7	41.3	1.2	2.1
NM_015254	Kinesin family member 13B	KIF13B	13.0	24.5	39.4	1.9	3.0
AL110249	Chromosome 20 open reading frame 194	C20orf194	13.4	39.0	29.7	2.9	2.2
AF208502	Early B-cell factor	EBF	12.5	21.1	28.5	1.7	2.3
AW007221	Solute carrier family 13 (sodium/sulfate symporters), member 4	SLC13A4	12.3	9.6	27.8	0.8	2.3
AB007458	TP53 activated protein 1	TP53AP1	12.6	22.2	26.2	1.8	2.1
AV713913	Osteopetrosis associated transmembrane protein 1	**OSTM1**	9.8	16.5	21.3	1.7	2.2
BF339201	THAP domain containing 6	THAP6	6.0	14.0	20.6	2.3	3.4
AK000455	Hypothetical gene MGC16733 similar to CG12113	MGC16733	7.3	16.6	18.8	2.3	2.6
AW974816	–	–	2.2	16.0	17.2	7.2	7.7
AK025325	Transcribed locus, moderately similar to NP_689573.2 zinc finger protein 573	–	7.3	11.4	16.2	1.6	2.2
NM_021192	Homeo box D11	**HOXD11**	5.3	16.2	15.8	3.0	3.0
NM_022169	ATP-binding cassette, sub-family G (WHITE), member 4	ABCG4	7.0	10.5	15.7	1.5	2.2
R62907	Disabled homolog 2, mitogen-responsive phosphoprotein (*Drosophila*)	DAB2	7.7	13.0	15.5	1.7	2.0
NM_002661	Phospholipase C, gamma 2 (phosphatidylinositol-specific)	PLCG2	7.3	12.3	15.3	1.7	2.1
BG393032	Solute carrier family 13 (sodium/sulfate symporters), member 4	SLC13A4	6.4	6.7	15.1	1.0	2.3
BC002794	Tumor necrosis factor receptor superfamily, member 14	TNFRSF14	6.2	11.3	13.6	1.8	2.2
BC042908	KIAA0690	KIAA0690	5.6	7.4	13.5	1.3	2.4
AW451961	Adenylate cyclase activating polypeptide 1 (pituitary) receptor type I	**ADCYAP1R1**	4.3	11.7	13.2	2.7	3.1
AI863264	Glypican 2 (cerebroglycan)	**GPC2**	5.3	7.2	13.2	1.3	2.5
AF130050	ACA47 scaRNA gene	-	5.6	9.5	12.9	1.7	2.3
AK022326	Hypothetical gene supported by AK022326	-	6.1	12.7	12.9	2.1	2.1
AK021807	Low density lipoprotein receptor-related protein 11	LRP11	5.9	6.2	12.8	1.0	2.2
AU155415	Kallikrein 7 (chymotryptic, stratum corneum)	KLK7	5.6	13.5	12.7	2.4	2.3
BF673779	Hypothetical protein FLJ30834	FLJ30834	5.5	6.3	12.3	1.1	2.2
AV646335	–	–	2.6	13.0	11.2	5.0	4.3
BC040600	–	–	5.0	5.4	10.6	1.1	2.1
AI131035	–	–	5.1	9.2	10.5	1.8	2.1

C, vehicle control; D, 5α-dihydrotestosterone; Ex, exemestane. Genes that performed quantitative RT-PCR were described in bold style.

Microarray/clustering analysis

In hFOB cells, the hierarchical clustering analysis contains 430 genes which demonstrated expression ratios above 2.0-fold and below 0.5-fold compared with vehicle control cells after 12 h of each gene treated with 10^{-8} M E2, 10^{-8} M DHT, or 10^{-7} M EXE. The expression profiles of EXE treated cells were closely related to those of DHT (Fig. 5). In this study, we focused on 35 genes (Table 3a), which were all up-regulated twice or more than control. In this group, we further focused on 5 genes, B-Myb 2 (MYBL2), osteopetrosis associated transmembrane protein 1 (OSTM1), homeo box D 11 (HOXD11), adenylate cyclase activating polypeptide 1 receptor (ADCYAP1R1), and glypican 2 (GPC2) which are all considered to play important roles in EXE or DHT induced cell proliferation. We therefore examined whether these 5 genes were increased by EXE or DHT treatments using quantitative RT-PCR in hFOB cells. We also examined the validation of results of microarray analysis obtained in hFOB cells in Saos-2 and MG-63 cells.

Validation of microarray analysis using quantitative RT-PCR

In hFOB cells, all of these 5 genes described above were significantly increased by 10^{-7} M EXE treatment, and 3/5 genes (except for OSTM1 and GPC2) were also significantly increased by 10^{-8} M DHT treatment. HOXD11 and ADCYAP1R1 genes increased by both EXE and DHT were significantly diminished by OHF (5×10^{-6} M) treatment (Figs. 6A–C).

The similar results of changes of MYBL2 expression were also obtained in both Saos-2 and MG-63 treated with EXE and DHT, respectively (Fig. 6A). In addition, the results of HOXD11 expression in hFOB were equivalent to those in Saos-2 but not in MG-63 treated with EXE and DHT (Fig. 6B). Other genes induced by treatment of EXE and DHT in hFOB such as OSTM1, GPC2, and ADCYAP1R1 were not changed in both Saos-2 and MG-63 cells treated with EXE and DHT, respectively (data not present). AI-I or AGM treatment did not increase all of these genes expression in hFOB (data not present).

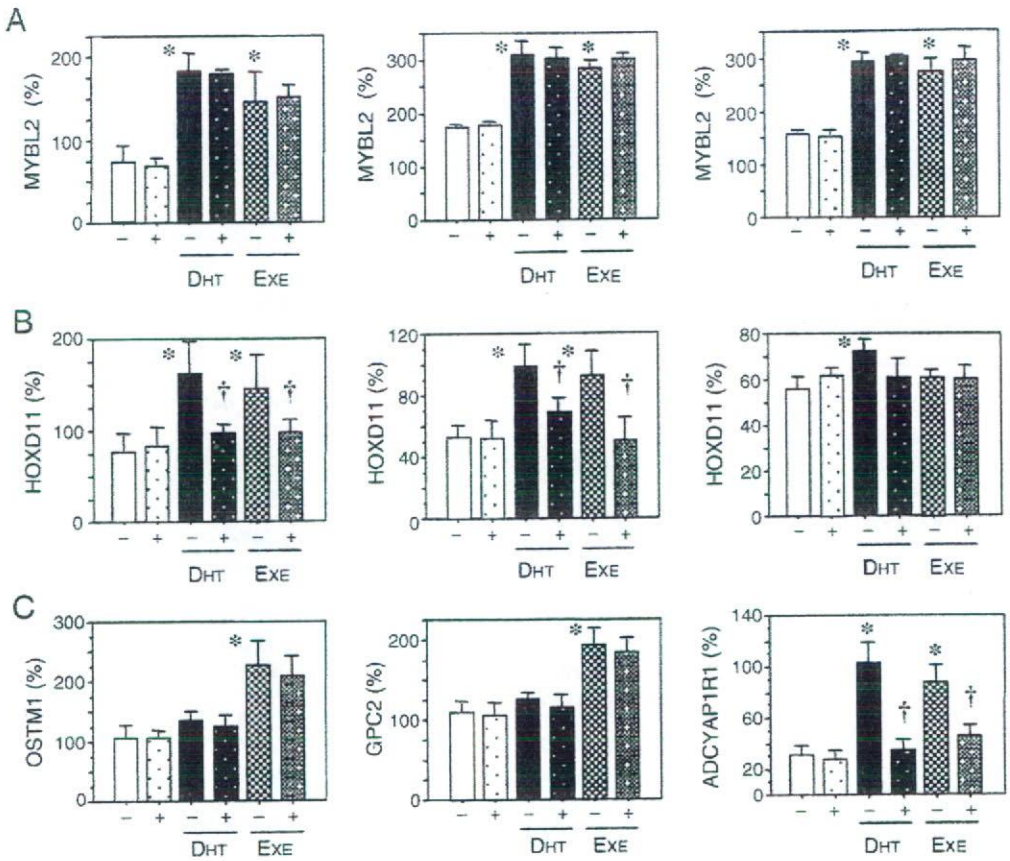

Fig. 6. Validation of microarray analysis. (A) Expression levels of MYBL2 in hFOB (left), Saos-2 (middle), and MG-63 (right). (B) Expression levels of HOXD11 in hFOB (left), Saos-2 (middle), and MG-63 (right). (C) Expression levels of OSTM1, GPC2, and ADCYAP1R1 in hFOB. DHT: 10^{-8} M 5α-dihydrotestosterone, EXE: 10^{-7} M Exemestane, with (+) or without (−) hydroxyflutamide, $p<0.05$ vs. control (*) or without hydroxyflutamide (†).

Analysis of osteoblast growth-related genes

Results of microarray analysis in hFOB cell demonstrated that osteoblast growth-related genes [24,25] such as COL1A1, SMAD1, SMAD5, SPARC, and RUNX2 were all up-regulated by exemestane (10^{-7} M) treatment but the degrees of increment were all under 2-fold (Table 3b). In this microarray analysis, other expression levels of previously reported osteoblast-related genes were not altered.

In hFOB cells, the validation analysis of these genes described above using quantitative RT-PCR (Fig. 7) demonstrated that 4/5 genes (except for COL1A1) were significantly increased by 10^{-7} M EXE treatment, and 4/5 genes (except for SMAD1) were also significantly increased by 10^{-8} M DHT treatment. The increased expression of the SMAD1, SMAD5, and SPARC genes by EXE or DHT, was significantly diminished by OHF (5×10^{-6} M) treatment. There were no effects of OHF pretreatment on the increased expression levels of RUNX2 that had occurred after both EXE and DHT treatments. Both AI-I and AGM treatment could not increase all of these genes expression in hFOB (data not present).

In Saos-2 cells, 4/5 genes (except for RUNX2) were significantly increased by 10^{-7} M EXE treatment, and 3/5 genes (except for RUNX2 and SMAD1) were also significantly increased by 10^{-8} M DHT treatment. The increment of the COL1A1, SMAD5, and SPARC genes expression by EXE or DHT, was significantly diminished by OHF (5×10^{-6} M) treatment. All of these 5 genes did not change in MG-63 cells treated with EXE or DHT, respectively (data not present).

Immunohistochemistry of AR

Marked AR immunoreactivity was detected in the nuclei of osteoblasts or lining cells but not in osteoclasts in four cases (Fig. 8). In these four cases, AR immunoreactivity was also detected in osteocytes and condrocytes. In one case, there was no immunoreactivity in all types of bone cells.

Discussion

In the clinical study of EXE compared to placebo administrated for two years [26,27], EXE modestly enhanced bone loss from the femoral neck without significant influence on lumber bone loss despite a marked systemic estrogen depletion. Furthermore, the risks of clinical bone fractures are considered to be lower with EXE treatment than that seen with non steroidal AIs [27,28], though it is also important to recognize that EXE has not been shown to significantly increase the amount of bone mass in various clinical studies of breast cancer patients [26,27]. The relative protective effect of EXE, a